The Remote Sensing of Tropospheric Composition from Space

Editors:
John P. Burrows
Ulrich Platt
Peter Borrell

Pages 259 to 314
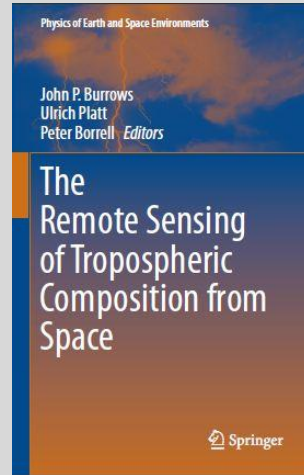
Chapter 6

Retrieval of Aerosol Properties

Gerrit de Leeuw, Stefan Kinne, Jean-Francois Léon, Jacques Pelon, Daniel Rosenfeld, Martijn Schaap, Pepijn J. Veefkind, Ben Veihelmann, David M. Winker and Wolfgang von Hoyningen-Huene

Chapter 6
Retrieval of Aerosol Properties

Gerrit de Leeuw, Stefan Kinne, Jean-Francois Léon, Jacques Pelon, Daniel Rosenfeld, Martijn Schaap, Pepijn J. Veefkind, Ben Veihelmann, David M. Winker and Wolfgang von Hoyningen-Huene

6.1 Introduction

Atmospheric aerosol is a suspension of liquid and solid particles in air, i.e. the aerosol includes both particles and its surrounding medium; in practice aerosol is usually referred to as the suspended matter, i.e. the particles or the droplets, depending on their aggregation state. Particle and droplet radii vary from a few nm to more than

G. de Leeuw (✉)
Climate Change Unit, Finnish Meteorological Institute, Helsinki, Finland
and
Department of Physics, University of Helsinki, Helsinki, Finland
and
TNO Environment and Geosciences, Utrecht, The Netherlands

S. Kinne
MPI-Meteorology, Hamburg, Germany

J.-F. Léon
LOA, Lille, France

J. Pelon
Université Pierre et Marie Curie, Paris, France

D. Rosenfeld
The Hebrew University of Jerusalem, Jerusalem, Israel

M. Schaap
TNO Environment and Geosciences, Utrecht, The Netherlands

P.J. Veefkind
Royal Netherlands Meteorological Institute (KNMI), De Bilt, The Netherlands

B. Veihelmann
ESA/ESTEC, European Space Agency, Noordwijk, The Netherlands

D.M. Winker
NASA Langley Research Center, Hampton, USA

W. von Hoyningen-Huene
Institute of Environmental Physics, University of Bremen, Bremen, Germany

100 μm (Seinfeld and Pandis 1998). Aerosol particles are distinctly different from cloud droplets as regards their physical properties and aggregation state.

The particles can be directly emitted into the atmosphere (e.g. sea spray aerosol, dust, biomass burning aerosol, volcanic ash, primary organic aerosol) or produced from precursor gases (e.g. sulfates, nitrates, ammonium salts, secondary organic aerosol). The total aerosol mass is dominated by particles produced from the surface by natural processes, in particular sea spray aerosol and desert dust. Anthropogenic emission of both primary particles and precursor gases contributes appreciably to the total aerosol load (Andreae and Rosenfeld 2008).

A complete description of aerosol properties requires a multitude of parameters, such as particle size, particle concentration as function of size (particle size distribution), which can vary by roughly ten orders of magnitude, particle shape, and chemical composition. Each of these parameters depends on the type of the sources, chemical reactions in the atmosphere, and removal processes such as wet deposition (induced by precipitation,) and dry deposition (gravitational fallout and turbulence). The chemical composition determines the complex refractive index of the aerosol, which in turn (together with particle shape) determines their optical properties. Chemical composition implicitly includes the amount of water in a particle, which in turn is determined by its hygroscopicity and by the ambient relative humidity (RH). Often aerosol size distributions, which describe the aerosol concentration as function of particle size, are modelled as lognormal size distributions defined by the effective mean radius and standard deviation, whereas the amplitude varies with aerosol concentration. For such conditions the aerosol number concentrations N_i are distributed over a range of aerosol particle radii r_i following an n-mode lognormal distribution:

$$\frac{dN}{d\ln r} = \sum_{i=1}^{n} \frac{N_i}{(2\pi)^{1/2} \ln \sigma_i} \exp\left(-\frac{\left(\ln r_i - \ln \bar{r}_{gi}\right)^2}{2\ln^2 \sigma_i}\right) \tag{6.1}$$

where $\bar{r}_{gi}$ is the geometric mean radius and σ_i is the geometric standard deviation of the i-th lognormal mode. Bimodal size distributions are often assumed. Particles are often hygroscopic; therefore the aerosol radius r can be specified in its dry state (r_d), at a relative humidity RH of 80% (r_{80}), or any other RH.

The complex refractive index m is expressed as $m = n - ik$, where the real part n specifies the refraction in a medium due to the change in the speed of light with respect to that in vacuum, and k determines the absorption; both constants depend on the wavelength of the propagating light beam and on the properties of the medium. Both m and k need to be specified as a function of wavelength to calculate the optical properties. For this purpose, particles are generally assumed to be spherical allowing the application of Mie theory (Mie 1908, Chapter 1) to compute extinction and absorption coefficients and the scattering phase function. The latter describes the angular dependence of the scattering. The sphericity assumption is not appropriate for dust (or other solid) particles, which require more sophisticated methods to determine their optical properties (Dubovik et al. 2006). Aerosol optical properties determine the

scattering and absorption of solar radiation, which in turn determine the effects of aerosol on climate and provide a way to observe aerosol properties using electro-optical instruments. Some of these can be used *in situ*, on the ground or in aircraft, whereas others can be used on platforms such as satellites or aircraft and thereby provide the means for the remote sensing of aerosols, which is the topic of this chapter.

Aerosols play an important role in climate and air quality. The impact on climate is induced by the scattering and absorption of incoming solar radiation. The combined effect of scattering and absorption is termed the direct radiative effect of aerosols on climate. Aerosol scattering reduces the amount of incoming radiation reaching the Earth surface and hence constitutes cooling. The net effect of aerosols is cooling which partly offsets the impact of the global warming caused by the absorption by greenhouse gases. Since aerosol particles are often hygroscopic they can act as cloud condensation nuclei (CCN). As the amount of precipitable water available for condensation on CCN is often limited in the atmosphere, an increase in CCN, and thus increased cloud droplet concentrations, results in smaller cloud droplet sizes and enhanced cloud albedo. This has been termed the first indirect effect of aerosols on climate. The smaller cloud droplets precipitate more slowly and evaporate faster, which affects precipitation. This is termed the second indirect effect on climate. Some aerosols contain contaminants, which absorb strongly in the visible in addition to the absorption of liquid water. Overall our understanding of the effects of aerosols on climate is poor (IPCC 2007).

Aerosols have a large impact on our understanding of air quality as they reduce visibility and increase the amount of diffuse radiation. The latter has recently been shown to have impacts on the land carbon sink through its effect on photosynthesis (Mercado et al. 2009). In addition the occurrence of fine particle matter impacts on human health, which is another important aspect of air quality. Concentrations of fine particulate matter are commonly expressed as the mass of dry aerosol particles, PM10 or PM2.5, where 10 (2.5) refers to the maximum aerosol diameter, in μm, for dry particles contributing to the measured mass.

The data from instruments aboard satellites provide a unique method to observe aerosol properties with the same retrieval technique and the same instrument from local to regional to global scales (Kaufman et al. 2002). Instruments used for aerosol measurements from space, see Kokhanovsky and de Leeuw (2009) for an overview, were often not specifically designed for this task, but nevertheless provide valuable information which is complementary to that from instruments dedicated to the remote sensing of aerosols. Algorithms have been developed to determine aerosol properties from satellite observations of back scattered solar radiation.

A brief description of the history of aerosol observations from space is given by Lee et al. (2009). One of the first retrievals of aerosol optical depth from space-borne measurements of the spectral intensity of the reflected solar light was performed using observations from the MSS (Multi Spectral Scanner) on board the Earth Resources Technology Satellite (ERTS-1) (Griggs 1975; Mekler et al. 1977). The first operational aerosol products were generated using data from the AVHRR (Advanced Very High Resolution Radiometer) (Stowe et al. 2002) on

board the TIROS-N satellite launched in 19th October 1978. The Nimbus-7, launched in 25th October 1978, carrying the Stratospheric Aerosol Measurement instrument (SAM) (McCormick et al. 1979) and the Total Ozone Mapping Spectrometer (TOMS) (Torres et al. 2002). Thus the retrieval of aerosol properties from satellite-based observations started some 3 decades ago. Initially, retrievals were obtained only for measurements over water; aerosol retrieval results over land have started to become available on a regular basis only in the last decade.

AVHRR and TOMS have provided a long term aerosol product over the ocean spanning a period of roughly 3 decades. A long term aerosol product over land, since 1995, is produced using ATSR-2 (Along Track Scanning Radiometer) (Veefkind et al. 1998) and AATSR (Advanced Along Track Scanning Radiometer) measurements (Grey et al. 2006; Thomas et al. 2007), with the prospect of a longer time series using data from the SLST (Sea and Land Surface Temperature) planned for launch in 2013, as part of Sentinel-3. The long time series over oceans provide information on trends or changes in the last 30 years (Mishchenko et al. 2007). The aerosol data product delivered from TOMS was initially the Absorbing Aerosol Index, a measure for the presence of absorbing aerosol. Subsequently an algorithm was developed to retrieve the aerosol optical depth (AOD, the column-integrated extinction, see Section 6.3) (Torres et al. 1998; 2002).

The launch of lidars in space has added a new dimension to satellite observation of aerosol properties by providing information on the vertical distribution of aerosols and clouds. The first lidar measurements of aerosol back scattering from space were made by the instrument LITE (LIdar in space Technology Experiment) (Winker et al. 1996). LITE is a three-wavelength backscatter lidar which flew on the space shuttle Discovery in September 1994. LITE was operated for 53 h and provided views of multilayer cloud structures and observations of the distribution of desert dust, smoke, and other aerosols. LITE also provided the first global observations of planetary boundary layer height (http://www.lite.larc.nasa.gov/). A second lidar instrument, GLAS (Geoscience Laser Altimeter System) was launched in January 2003 as part of NASA's Earth Observing System (EOS) and was the sole instrument on ICESat (Ice, Cloud, and land Elevation Satellite). One of the secondary objectives of GLAS includes the measurement of cloud and aerosol height profiles (Zwally et al. 2002) (http://icesat.gsfc.nasa.gov/index.php). A dedicated aerosol and cloud lidar, CALIOP (Cloud-Aerosol Lidar with Orthogonal Polarization), was launched on CALIPSO (Cloud Aerosol Lidar and Infrared Pathfinder Satellite Observations) in April 2006. CALIPSO is part of the A-train, a constellation of satellites with instruments designed to study aerosols and clouds: Cloudsat, PARASOL (the follow up of POLDER – POLarization and Directionality of the Earth's Reflectances), MODIS (Moderate Resolution Imaging Spectroradiometer) and OMI (Ozone Monitoring Instrument).

A measure of the effect of aerosols and clouds on the Earth's radiative balance is provided by the direct measurement of the upwelling radiation at the top of the atmosphere. However, the effects of the surface and atmospheric constituents need to be separated. This is accomplished by retrieval algorithms, which provide information on the AOD at the measured wavelengths. More sophisticated research

algorithms, see Kokhanovsky and de Leeuw (2009) for a recent review, provide aerosol microphysical properties, such as effective radius, ratio of fine to coarse fraction, single scattering albedo and composition. Unlike ground-based and airborne measurements, instruments aboard satellites provide information over a large area with up to daily global coverage for polar orbiting satellites. Geostationary satellites provide high temporal resolution (15 min) over a large area and hence allow for studies of the diurnal evolution of aerosol properties, as well as the interaction between clouds and aerosols.

The information on aerosols is in the atmospheric reflectance, also referred to as path radiance. Before the aerosol information can be retrieved using algorithms that fit models describing the radiative transfer through the atmosphere with different types of aerosols, the path radiance needs to be separated from the effects due to clouds and surface reflection. Clouds are bright and even small traces of clouds can contaminate the atmospheric signal (Chapter 5). It is therefore important to detect accurately the occurrence of clouds within a ground scene. This is one of the major issues for aerosol retrieval. In particular the presence of sub-visible clouds and high cirrus may contaminate the signal, as well as the distinction between clouds and aerosol near cloud edges (Koren et al. 2007). Another major issue for the retrieval of aerosol data products is the removal of land surface effects from the top of the atmosphere (TOA) radiation. For single-view instruments this is typically dealt with by using assumptions about the reflectance at wavelengths in the near infrared and the spectral dependence of the reflectance by specific surfaces, or by using a surface reflectance data base. When multiple views are available, the surface contribution to the TOA radiation can be eliminated explicitly. The remaining TOA radiation for cloud-free sky, after elimination of the surface contributions, is the atmospheric path radiance, which is compared with the path radiance computed using a radiative transfer model. By minimizing the difference between computed and observed radiances, the AOD can be determined. When more than one wavelength is available, the minimization should be made using all available wavelengths, to determine the most likely aerosol type (or mixture) in the atmospheric column.

Instrumental characteristics required for aerosol retrieval are multiple wavelengths, multiple viewing angles and polarization. PARASOL (Polarization and Anisotropy of Reflectances for Atmospheric Sciences coupled with Observations from a lidar) is an instrument that combines all of these. MISR (Multiangle Imaging SpectroRadiometer) has multiple viewing angles and multiple wavelengths. AATSR has two views and multiple wavelengths. MODIS, MERIS (MEdium Resolution Imaging Spectrometer) and OMI have multiple wavelengths. Therefore the algorithms for each of these instruments are different, and the algorithms for a single instrument may be very different (see Kokhanovsky and de Leeuw (2009) for descriptions of three algorithms used for aerosol retrieval using AATSR data). The algorithms differ in the way they deal with the surface reflectance, which is an important issue over land surfaces. They also differ in the way they screen clouds, and in the aerosol models used in the retrieval. These issues are treated in Sections 6.6 to 6.11. An overview of pertinent characteristics of instruments discussed in this chapter is presented in Appendix A.

The use of aerosol data products derived from instrumentation aboard satellites contributes to our understanding and documenting of regional and global aerosol and cloud properties, including their variations, as well as aerosol-cloud interactions. It provides a 4-D distribution of aerosol and cloud properties on regional and global scales, using data from radiometers (multi-spectral, multi-angle and polarization) which provide the spatial distribution, and lidar data from CALIOP which provide the vertical distribution, all of these as a function of time which allows for following the evolution of the aerosol properties.

These instruments are of experimental nature, and hence have a limited lifetime, in contrast to the operational satellites provided by the METEOSAT (Meteorological satellite – geostationary) and MetOp (Meteorological Operational satellite programme) series of instruments and the GMES (Global Monitoring for Environment and Security) operational system that is developed by ESA (European Space Agency) and EUMETSAT (European Organisation for the Exploitation of Meteorological Satellites). The geostationary instrument SEVIRI (Spinning Enhanced Visible and Infrared Imager – flying on METEOSAT Second Generation, MSG) has the advantage of very high temporal resolution. AATSR flying on ENVISAT (ENVIronmental SATellite) does not provide global coverage in one day, as it has a limited swath, but as indicated above, it is intended to continue the current time series of 15 years (1995–2010) and thus provide more than 20 years of aerosol properties over land.

A description of aerosol retrieval over land using current instrumentation is provided in Kokhanovsky and de Leeuw (2009). This book describes the state of the art about the retrieval of aerosol data products over land, and comprises a series of articles solicited to represent instruments that are currently used for this purpose in a sun synchronous orbit (MODIS, MISR, POLDER, AATSR, MERIS) and SEVIRI which is in a geostationary orbit. For AATSR three different retrieval algorithms, based on different principles, were presented. Tables providing the general characteristics of instruments currently used for aerosol retrieval can also be found in the introduction to the book (de Leeuw and Kokhanovsky 2009).

In this chapter we provide supplementary information about the current state of the art of aerosol retrieval using CALIPSO, POLDER, AATSR, MODIS, OMI and MERIS observations and algorithms that have been developed for these instruments. Brief descriptions of these instruments and their data products are provided in Sections. 6.6 to 6.11. In addition, examples are presented describing applications of satellite data for air quality, climate and aerosol-cloud interaction studies.

6.2   Aerosol Retrieval Algorithms

Aerosol retrieval is based on the comparison of the radiation received by an instrument at TOA with that calculated using a radiative transfer model for the same geometry and atmospheric conditions, for a range of aerosol models. The best fit model is selected to provide the retrieval solution, i.e. AOD and other aerosol

properties. Aerosol retrieval algorithms utilize data obtained from observations with instruments mounted on a satellite in a certain orbit, with a certain viewing angle and for a solar zenith angle which varies with the season and the time of day. Aerosol particles scatter light in different directions with an angular distribution that depends on particle size, shape, and chemical composition, and is described by the scattering phase function. The intensity of the scattered light can vary by several orders of magnitude depending on particle size. Any aerosol retrieval algorithm uses the angular dependence of the aerosol scattering and therefore needs to take the specific geometry into account. However, aerosol properties can only be retrieved for cloud-free scenes because scattering by cloud droplets not only overwhelms the aerosol signal, but also has different angular dependence.

Therefore, the first step in any retrieval algorithm is cloud screening. Several criteria may be applied for cloud detection (Ackerman et al. 1998). The retrieval of cloud properties is discussed in Chapter 5. Cloud screening methods are based on a variety of principles, including thresholding of the radiances measured at wavelengths in the near and thermal infrared, the wavelength dependence of the radiances for pairs of channels at wavelengths in the visible to the thermal infrared, the analysis of spatial and temporal patterns, the use of the O_2 A-band, and also the synergistic use of other instruments, including lidars. An example of the application of cloud screening is presented in Section 6.8.

The next problem for clear sky measurements is to account for the land surface contribution to the TOA reflectance. Several different methods are implemented in retrieval algorithms, depending on instrument properties. This is discussed in Sections 6.7 to 6.11 for the individual instruments treated here. After correction for the surface contribution to the TOA radiance, the path radiance, which includes contributions from molecular scattering and absorption, remains. To account for molecular effects for the given sun-satellite geometry properly, a radiative transfer model (RTM) is applied to a set of observation and illumination geometries for a wide range of situations. This is referred to as forward modelling; the retrieval is referred to as inverse modelling.

Radiative transfer calculations are usually time consuming (see Katsev et al. (2009) for an example of the use of a fast radiative transfer code as part of the retrieval algorithm) and are used outside the actual retrieval algorithm to prepare look up tables (LUTs) for a wide variety of situations; these include the viewing geometry expressed by the solar and viewing zenith angles and relative azimuth angle, the wavelengths that are used in the retrieval, a series of reference AOD levels from very low to very high, and other relevant parameters depending on the instrument characteristics used in the retrieval, together with atmospheric information such as surface pressure. The angles and AOD levels are varied in discrete steps. For each combination, forward calculations are made for a series of aerosol models (see Section 6.4) and the results are stored in LUTs. A LUT is thus prepared for each aerosol model and contains parameters such as AOD, single scattering albedo ω, spherical albedo, total and diffuse transmittance along the atmospheric path (downward and upward), total and diffuse downward transmittance of the atmospheric column, surface downward reflectance, and path reflectance. Each of

these parameters depends on one or more of the input parameters. The LUTs are used in the retrieval step to speed up the processing. The parameters contained in the LUT are interpolated between the discrete levels to provide for the actual situation, in particular the viewing geometry. Examples of LUT contents are presented in Sections 6.7 and 6.9.

The LUTs are usually prepared using vector radiative transfer calculations for a set of aerosol models which are representative for a certain area (Kaufman et al. 2001; Dubovik et al. 2002; Levy et al. 2007a; 2007b). Ideally, the algorithm must have the ability to select the most appropriate aerosol model or mixture of aerosol models. In many cases, however, aerosol type selection is based on climatology (Levy et al. 2007a; Curier et al. 2008). Such climatologies can be derived from observations (Dubovik et al. 2002; Levy et al. 2007a) or from results from transport models for the area of interest (Curier et al. 2008). In the future, it may be possible to use transport model forecasts (Verver et al. 2002) to constrain the retrieval.

6.3 Aerosol Optical Parameters

Optical properties that are important for the remote sensing of aerosols, and applications for climate and air quality are the extinction and backscatter coefficients, the scattering phase function and the single scattering albedo. These parameters are derived from the aerosol particle size distribution and the refractive index, which is determined by the chemical composition. Moreover, both the aerosol particle size and the chemical composition vary with RH. Chemical and physical properties of aerosols change during their atmospheric lifetime due to a variety of processes (Seinfeld and Pandis 1998), and the RH varies in space and time, so the optical properties change horizontally, vertically, and in time.

When a light beam hits a medium containing aerosol the intensity is reduced due to scattering and absorption by the particles. This is described by the Lambert–Beer law:

$$I(\lambda) = I_o(\lambda) \exp(-\int_0^h b_{ext}(\lambda)dz), \qquad (6.2)$$

where I_o and I are the intensities of the incoming and exiting light beams, respectively, with wavelength λ, z is the position in the medium with thickness h and b_{ext} is the aerosol extinction coefficient, which is given by the sum of the scattering and absorption coefficients, b_{scat} and b_{abs} ($b_{ext} = b_{scat} + b_{abs}$). These coefficients are determined by the product of the particle size distribution $n(r)$ and the extinction, scattering or absorption efficiency, $Q_{ext}(r, m, \lambda)$, $Q_{scat}(r, m, \lambda)$, $Q_{abs}(r, m, \lambda)$, respectively. For scattering:

$$b_{scat}(\lambda) = \int_{r_1}^{r_2} \pi r^2 n(r) Q_{scat}(r, m, \lambda)dr, \qquad (6.3)$$

The particle size distribution is a function that describes the concentrations of the aerosol particles as function of radius r (see Eq. 6.1 for a possible formulation). The scattering efficiency for a particle with radius r and complex refractive index $m = n-ik$, at wavelength λ, is given by:

$$Q_{ext}(r,m,\lambda) = C_{ext}(r,m,\lambda)/A(r), \tag{6.4}$$

where $C_{ext}(r, m, \lambda)$ is the extinction cross section and A is the geometric area of that particle. Similar expressions apply to $Q_{scat}(r, m, \lambda)$ and $Q_{abs}(r, m, \lambda)$. The single scattering albedo ω is defined as the ratio of the scattering and extinction efficiencies:

$$\omega(\lambda) = \frac{Q_{scat}(\lambda)}{Q_{ext}(\lambda)}. \tag{6.5}$$

The single scattering albedo is 1 for non-absorbing particles and common values are around 0.97 (0.95–1.0), but much lower values are observed in strongly polluted areas with large amounts of absorbing aerosol (e.g. emitted from forest fires and other combustion processes). Ground-based measurements of absorption and extinction are most reliable in providing such data, although research is needed to improve accuracy and reproducibility. Satellite data of the single scattering albedo are sparse and usually indirectly derived.

The extinction cross section is given by:

$$C_{ext}(r,m,\lambda) = C_{scat}(r,m,\lambda) + C_{abs}(r,m,\lambda) \tag{6.6}$$

and

$$C_{scat}(r,m,\lambda) = I_{scat}(\lambda)/I_o(\lambda) \tag{6.7}$$

with a similar expression for $C_{abs}(r,m,\lambda)$.

Similar equations apply for the aerosol scattering and absorption coefficients and efficiencies, note that $\int_0^h b_{ext}(\lambda)dz = \tau_{aer}(\lambda)$, where $\tau_{aer}(\lambda)$ is the AOD of the layer with depth h, also often called aerosol optical thickness (AOT), which is the primary parameter retrieved by satellites. The wavelength dependence of $\tau_{aer}(\lambda)$ is expressed by the Ångström relationship:

$$\tau_{Aer}(\lambda) = \beta \cdot \lambda^{-\alpha_A} = \tau_{Aer}(\lambda_{ref}) \cdot \left(\frac{\lambda}{\lambda_{ref}}\right)^{-\alpha_A}, \tag{6.8}$$

where β is the AOD at the reference wavelength λ_{ref} (usually taken at 1 μm) and α_A is the Ångström parameter evaluated for the wavelength pair λ_1 and λ_2. Typical values for α_A are in the range 1–2.

For the retrieval of aerosol properties from satellite observations, with a range of illumination and observation angles, information on the angular distribution of the

scattering intensity, which is described by the scattering phase function $P(\theta,\alpha,m,\lambda)$, is required:

$$P(\theta, \alpha, m, \lambda) = F(\theta, \alpha, m, \lambda) / \int_0^\pi F(\theta, \alpha, m, \lambda) \sin \theta d\theta \qquad (6.9)$$

where θ is the scattering angle and α ($=2\pi r/\lambda$) is the size parameter that accounts for the dependence of optical effects of aerosols on their size relative to the wavelength of the incoming light. In all of the above, equations which depend on both r and λ can be replaced by their dependence on α.

Other parameters often encountered are the asymmetry parameter g (see Chapter 5) which provides a measure for the major scattering direction and is given by:

$$g(\lambda) = \frac{1}{2} \int_0^\pi \cos \theta P(\theta, \lambda) \sin \theta d\theta, \qquad (6.10)$$

For light scattered totally at $\theta = 0°$, $g = 1$; $g = -1$ for light scattered totally at $\theta = 180°$ and $g = 0$ for isotropically scattered light. The hemispheric backscatter ratio is given by:

$$b(\lambda) = \frac{\int_{\pi/2}^\pi P(\theta, \lambda) \sin \theta d\theta}{\int_0^\pi P(\theta, \lambda) \sin \theta d\theta}. \qquad (6.11)$$

The transmission of a layer of air with thickness h is given by:

$$T(\lambda) = \frac{I(\lambda)}{I_0(\lambda)} = \exp(-\int_0^h b_{ext}(\lambda, z)dz). \qquad (6.12)$$

For the calculation of optical properties, it is commonly assumed that the aerosol particles are spherical, which implies that we can use Mie theory (Section 1.9.1). Mie theory is based on the exact solution of the Maxwell equations (Mie 1908) and program codes are readily available. Mie theory needs to be used for spherical particles with sizes on the order of the wavelength of the incident light, i.e. $\alpha \sim 1$. The angular scattering for much smaller particles is symmetric and can be calculated in the Rayleigh limit; the scattering by much larger particles can be calculated using the geometric approximation. Mie theory shows that scattered light has a strong forward lobe, with intensity strongly increasing with increasing particle size. Particles often are hygroscopic and thus absorb water vapour. Liquid particles are spherical for sizes in the optically active range.

For non-spherical particles Mie theory does not apply and approximations about the particle shape, e.g. treatment as spheroids, has to be made to calculate the phase

function. This is particularly important for the retrieval of desert dust which has irregular shapes and is non-hygroscopic. For instance, Dubovik et al. (2006) show examples of the application of spheroid models to account for aerosol particle non-sphericity in remote sensing of desert dust. Deviations from Mie theory occur in the scattering phase function for large scattering angles in both the forward and backward directions.

Light scattered by molecules and small aerosol particles is strongly polarized in a plane perpendicular to the scattering plane (the plane defined by the sun, the object being viewed and the observer) while light scattered by surfaces is only weakly polarized. This difference between the polarizing properties of aerosols and molecules as compared to surfaces is used by modern polarimetric remote sensing instruments to determine the amount, size and type of aerosols that are present above the surface. The intensity and polarization of light can be described by the Stokes vector $\boldsymbol{I} = (I, Q, U, V)$ where I is a measure of the intensity of the light, Q and U define the magnitude and orientation of the linearly polarized fraction of the light and V is a measure of the magnitude and helicity of the circular polarization. All four Stokes vector elements have the dimensions of intensity (Wm^{-2}). A detailed discussion of polarization and its use in aerosol remote sensing can be found in Cairns et al. (2009.)

6.4   Databases for Aerosol Properties

Databases for aerosol optical properties are available from analyses of the AERO-NET sun photometer network (Holben et al. 1998) derived from 8 years of worldwide distributed data for different aerosol types by Dubovik et al. (2002). Established procedures for maintaining and calibrating this global network of radiometers, cloud screening and inversion techniques facilitate the consistent retrieval of the optical properties of aerosols in locations with varying emission sources and conditions. The multi-year, multi-instrument observations show robust differentiation in both the magnitude and spectral dependence of the absorption for desert dust, biomass burning, urban, industrial and marine aerosols. The authors observed significant variability of the absorption for the same aerosol type due to different meteorological and source characteristics, as well as different emission characteristics.

This data base is particularly useful for application in satellite retrieval codes because similar parameters, such as column-integrated aerosol properties, are measured with both, but with much better accuracy and without interference from surface reflectance.

The application of the Dubovik data base to the retrieval of aerosol properties using AATSR observations has provided excellent results in areas with complicated aerosol composition, such as over the Indian Ocean where a transition has been observed from very polluted to very clean aerosol (Robles-Gonzalez et al. 2006), over Africa for biomass burning aerosol (Robles-Gonzalez and de Leeuw 2008) or over the desert for a mixture of fossil fuel and desert dust aerosol (de Leeuw et al.

2005). AERONET data were the basis for the MODIS Collection 5 (C005) aerosol retrieval algorithm (Levy et al. 2007a; 2007b).

Another aerosol data base that provides the parameters describing the aerosol models used in aerosol retrieval algorithms is the Global Aerosol Data Set (GADS). GADS is available from the software package OPAC (Optical Properties of Aerosols and Clouds) (Hess et al. 1998) (http://www.lrz-muenchen.de/~uh234an/www/radaer/opac.html). OPAC provides microphysical and optical properties of ten aerosol components including extinction, scattering and absorption coefficients, the single scattering albedo, the asymmetry parameter and the phase function. The computation of these parameters is based on the microphysical data (size distribution and spectral refractive index), assuming that the particles are spherical. Data are given for up to 61 wavelengths between 0.25 and 40 μm and up to 8 values of the relative humidity. The software package also facilitates the calculation of derived optical properties such as mass extinction coefficients, i.e. the extinction per unit of mass, specific for each aerosol type, and Ångström coefficients.

6.5 Instruments Used for the Retrieval of Aerosol Properties from Space

Data from instruments, which were not explicitly designed for the retrieval of aerosol, have been used to determine aerosol data products. For instance instruments like TOMS, GOME, SCIAMACHY and OMI were designed for the retrieval of trace gas concentrations and the purpose of AVHRR, SeaWiFS, MERIS and ATSR was to measure land/sea surface temperature. GLAS was primarily designed as an altimeter; LITE was set up as a technology experiment. However, data from each of these instruments has also been used for the retrieval of aerosol properties, with varied success. Dedicated instruments for aerosol retrieval are POLDER, MODIS, MISR and CALIOP. Ideally, a sensor should have the capability of observing multiple wavelengths from the UV to the TIR, multiple views, and polarization sensitivity. The combination of spectral polarization and multiple view measurements for a range of wavelengths is only available from the POLDER series of instruments (Deschamps et al. 1994), the latest of which is flying on PARASOL as part of the A-Train. The GLORY mission (Mishchenko et al. 2007) set to launch in February 2011 will carry the Aerosol Polarimetry Sensor (APS) which will collect accurate multi-angle photo-polarimetric measurements of the Earth along the satellite ground track over a wide spectral range extending from the visible to the short-wave infrared. The data from this instrument are expected to provide aerosol retrievals with a higher accuracy than available from current instruments. (A)ATSR and MISR combine two or multiple views, respectively, with multiple wavelengths.

Results from the last decade show that it is possible to obtain a useful set of aerosol parameters even without using the advanced multi-view instruments capable of

detecting the polarization state of the reflected solar light. In particular MODIS, which was designed for the measurement of aerosol and cloud properties, has been successful and is the most widely used for aerosol observations from space. The open data policy and accessibility of aerosol products has resulted in numerous publications from the use of MODIS data. Also the global coverage from two MODIS instruments (Terra descending, equator crossing time 10:30, and Aqua ascending, equator crossing time 13:30) ensure a high probability of obtaining useful data.

The parameters retrieved from measurements by instrumentation in space include the AOD at various wavelengths and its wavelength dependence expressed by the Ångström coefficient. Principle component analysis shows which other aerosol parameters could be retrieved using a dedicated aerosol instrument. These could include, for a bimodal aerosol model, the effective radius and effective variance, and the complex refractive index (both real and imaginary parts) for both modes. Examples are presented by Hasekamp and Landgraf (2005) for GOME-2 and Veihelmann et al. (2007) for OMI.

6.6 Retrieval of Aerosol and Cloud Parameters from CALIPSO Observations

CALIPSO is a satellite mission (see Appendix A) developed within the framework of a collaboration between NASA and the French space agency, CNES. CALIPSO provides unique measurements to improve our understanding of the role of aerosols and clouds in the Earth's climate system (Winker et al. 2003; 2009). The CALIPSO payload (see Table 6.1) consists of a two-wavelength polarization-sensitive lidar, and passive imagers operating in the visible and infrared spectral regions. The lidar profiles provide information on the vertical distributions of aerosols and clouds, cloud ice/water phase (via the ratio of signals in two orthogonal polarization

Table 6.1 Characteristics of the CALIPSO instruments

Characteristic	Value
CALIOP	
Wavelengths	532 nm, 1064 nm
Polarization	532 nm, ∥ and ⊥
Pulse energy	110 mJ each wavelength
Footprint	100 m
Vertical resolution	30–60 m
Horizontal resolution	333 m
WFC	
Wavelength	645 nm
Spectral bandwidths	50 mm
IFOV/swath	125 m/61 km
IIR	
Wavelengths	8.65 μm, 10.6 μm, 12.0 μm
Spectral resolution	0.6 μm–1.0 μm
IFOV/swath	1 km/64 km

channels) and a qualitative classification of aerosol size (via the wavelength dependence of the backscatter). Data from the three instruments are used together to measure the radiative and physical properties of cirrus clouds. CALIPSO is flown in a polar orbit as part of the A-Train constellation which, besides CALIPSO, consists of the Aqua, CloudSat, PARASOL and Aura satellites. The satellites of the constellation fly in a sun-synchronous polar orbit with a nominal ascending node equatorial crossing time of 13:30 local time. The orbit of CALIPSO is maintained to provide space-time coincidence with observations from the other satellites of the constellation. CALIPSO was launched at the end of April 2006, and data have been available from 13th June 2006.

CALIPSO has been designed to provide data to address three major objectives:

- To improve observationally-based estimates of direct and indirect aerosol radiative forcing;
- To improve the characterization of surface radiative fluxes and atmospheric heating rates; and
- To improve model parameterizations of cloud-climate feedbacks.

CALIPSO is also intended to address a number of secondary objectives, which include observing long range transport of pollutants, providing coincident measurements to validate and improve retrievals from other instruments within the A-train, and providing aerosol observations useful for atmospheric chemistry applications.

The Cloud-Aerosol Lidar with Orthogonal Polarization (CALIOP) provides global, vertically-resolved measurements of aerosol spatial distributions (Winker et al. 2007; 2009). It has the ability to perform height-resolved discrimination of aerosol into several types. As seen in Fig. 6.1, CALIOP can observe aerosol over bright surfaces and beneath thin clouds as well as in clear sky conditions. An elevated aerosol layer (yellow and red in the upper panel) between roughly 0.5°S, 12.9°E and 17°S, 8°E overlies a stratus deck (white and red). At the left edge of the plot, two aerosol layers can be seen at altitudes of about 2 km and 5 km. Depolarization signals (lower panel) allow the identification of smoke (depolarization less than 10%) from dust (depolarization greater than 10%). CALIOP also provides vertical profiles of single and multi-layer transmissive clouds. The Imaging Infrared Radiometer (IIR) and Wide Field Camera (WFC) data combined with lidar data are used to retrieve cloud emissivity and effective particle size. Lidar data is incorporated into a split-window retrieval algorithm to provide constraints to improve the retrieval performance.

6.6.1 The CALIPSO Science Payload

The CALIPSO payload consists of three nadir-viewing instruments: CALIOP, IIR and WFC. These instruments are designed to operate autonomously and continuously, although the WFC acquires science data only under daylight conditions. The
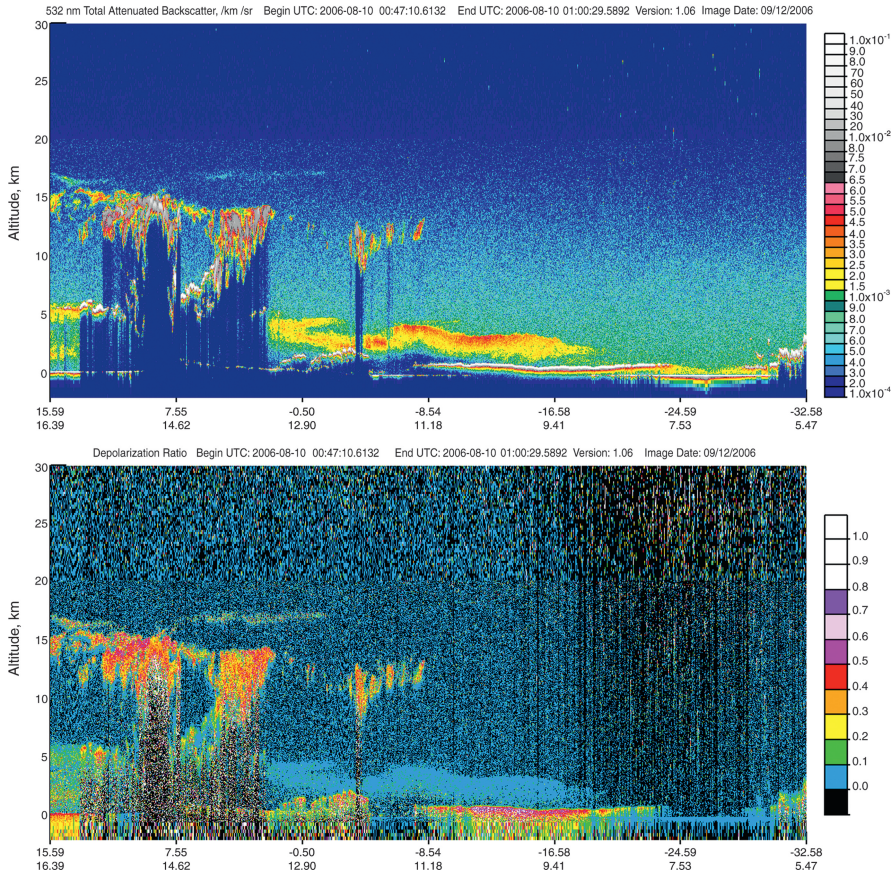
Fig. 6.1 CALIOP observations over west-central Africa. *Upper panel*: Calibrated 532 nm backscatter signals. *Lower panel*: Depolarization profiles from the ratio of the CALIOP 532 nm perpendicular and parallel return signals.

key characteristics of these instruments are listed in Table 6.1. The raw lidar data down-linked to the ground station has the vertical resolution given in Table 6.2.

6.6.2   CALIOP Data Calibration

The calibration algorithms are designed to accomplish two major functions. First, the determination of calibration coefficients for the three lidar channels, and second, the application of these calibration coefficients to produce attenuated backscatter profiles used in Level 2 processing. Determination of the calibration coefficients is basically a three-step process used to derive the Level 1B data products:

Table 6.2 Spatial Resolution of Down-linked Lidar Data

Altitude range	Horizontal resolution	Vertical resolution
30.1 km to 40 km	5.0 km	300 m (532 nm only)
20.2 km to 30.1 km	1.67 km	180 m
8.2 km to 20.2 km	1.0 km	60 m
−0.5 km to 8.2 km	0.33 km	30 m at 532 nm
		60 m at 1064 nm
−2.0 km to −0.5 km	0.33 km	300 m

(a) The calibration coefficient is determined for the 532 nm parallel channel (Powell et al. 2009). For the baseline approach, this is done by comparing the measured 532 nm parallel channel signal from the 30–34 km region to an estimate of the parallel backscatter coefficient computed from a modelled atmospheric density profile. The 30–34 km altitude range is chosen because there is little aerosol in that height range, especially at mid and high latitudes. At low latitudes there is a small bias due to the stratospheric background aerosol. The molecular backscatter coefficients can be estimated well, using knowledge of the molecular number density and theoretically derived estimates of the molecular backscatter cross section (Reagan et al. 2002).

(b) The 532 nm perpendicular channel is then calibrated relative to the calibration obtained for the parallel channel. There is not enough signal to calibrate the perpendicular channel using stratospheric molecular returns, because the depolarization of clear-air 180°-backscatter is only about 0.35%. The calibration is therefore transferred from the parallel to the perpendicular channel using data collected during the Polarization Gain Ratio (PGR) operation (Hunt et al. 2009).

(c) Calibration of the 532 nm parallel and perpendicular channels is then transferred to the 1064 nm channel. As with the 532 nm perpendicular channel, the signal from the 1064 nm channel in the mid-stratosphere is too low to provide a reliable calibration measurement. Transfer of calibration from the 532 nm channels to the 1064 nm channels is accomplished using the backscatter from properly chosen cirrus clouds. Because cirrus cloud particles are large, the ratio of the 532 nm and 1064 nm backscatter coefficients is approximately equal to 1. The 1064 nm calibration coefficient is determined by comparing the 1064 nm backscatter signal with the calibrated 532 nm cirrus backscatter measurements (Reagan et al. 2002).

6.6.3 Description of Available Data Products from CALIOP

The data products generated from the CALIOP measurements are produced according to a protocol which is similar to, but not exactly the same as, that established by NASA's Earth Observing System (EOS).

The data product levels for CALIPSO are reported in Table 6.3. They are defined below.

Table 6.3 CALIPSO product list

Data level	Data products	Production schedule
1b	Calibrated lidar profiles Calibrated IIR radiances Uncalibrated WFC radiances Meteorological profiles Lidar aerosol & cloud browse images	Data produced on 2-day lag following receipt of all required ancillary data (meteorological profiles). Archived and publicly available.
2a	Lidar backscatter profiles Aerosol layer height/thickness Cloud height/thickness	Data produced on 3-day lag thereafter. Archived and publicly available. Last reprocessing Dec. 2007/Jan. 2008.
2b	Aerosol extinction, optical depth Cloud extinction, optical depth Cloud ice/water phase Cloud emissivity (IIR)	First data released in January 2008
2c	Ice particle size (IIR)	First data released in January 2009

- *Level 0*: reconstructed, unprocessed instrument/payload data at full resolution; and with all communications artifacts, e.g. synchronization frames, communications headers, duplicate data removed.
- *Level 1B*: reconstructed, unprocessed instrument data at full resolution which is time-referenced, geo-located, corrected for instrument artifacts, and includes ancillary information processed to sensor units and archived as Level 1 data.
- *Level 2*: geophysical variables derived from Level 1 data, including those derived using measurements from multiple CALIPSO instruments.

The data products are archived upon the completion of the Level 1 processing and include profile products and calibration products.

6.6.4   CALIOP Retrieval Procedure for the Extinction Coefficient

The extinction coefficient determination requires several steps. The first one is the identification of the altitude of the scattering layer using the SIBYL (Selective Iterated Boundary Locator) algorithm (Vaughan et al. 2002; 2005; 2009). SIBYL scans lidar profiles throughout the troposphere and stratosphere, identifies regions of enhanced scattering, and records the location and simple characteristics of these atmospheric features.

Then the SCA (Scene Classification Algorithm (SCA (Liu et al. 2005; 2009), which is actually a set of algorithms, is used to classify these layers by type. It relies on a statistical analysis of observed parameters (Liu et al. 2004; 2009). In addition to being incorporated into the output data products, some of the type classifications performed by the SCA are also required by the hybrid extinction retrieval algorithm (HERA (Young et al. 2005; Young and Vaughan 2009)).

After SIBYL has found a region in a lidar profile, SCA first discriminates between cloud and aerosol and then determines the cloud or aerosol sub-type. Surface, subsurface and totally attenuated regions are also recorded in the Vertical

Feature Mask (VFM). If the region is a feature (cloud or aerosol) SCA then checks to see if the feature is lofted (if the molecular scattering signal is available both above and below the feature for feature layer transmittance retrieval). For a lofted feature, the SCA will derive the lidar ratio using the transmittance-constraint method (Fernald et al. 1972; Young 1995). For both lofted and non-lofted layers, the SCA will conduct a classification of feature types and assign a lidar ratio to the feature corresponding to the extinction processing in HERA. Note that if the feature is lofted and a lidar ratio can be derived using the transmittance method, the computed lidar ratio is selected; if the feature is non-lofted, a lidar ratio is selected based on the model corresponding to the identified feature type. Aerosol models were developed using data from AERONET (Omar et al. 2004; 2009).

For the feature classification, the SCA first determines whether the feature is tropospheric or stratospheric by checking the base altitude of the feature. The tropopause altitude is derived from ancillary data obtained from the Global Modelling and Assimilation Office (GMAO). If the feature base is lower than this altitude, the feature is classified as a tropospheric feature; otherwise, it is classified as a stratospheric feature. If a feature is tropospheric, further classifications (four algorithms) are conducted to sub-type the feature.

The SCA first determines whether a layer is cloud or aerosol, primarily using the layer mean value of the 532 nm attenuated backscatter coefficient, and the attenuated color ratio, which is the ratio of the mean attenuated backscatter coefficients measured at 1064 nm and 532 nm. If the layer is classified as cloud, the SCA will then determine whether it is an ice cloud or water cloud using the measured backscatter intensity and the depolarization ratio profiles, along with ancillary information such as layer height and temperature. The SCA will also use a combination of observed parameters and *a priori* information to select an appropriate extinction-to-backscatter ratio, or lidar ratio (Sa for aerosol layers, Sc for clouds), and multiple scattering function, $\eta(z)$ as defined by Platt (1973), required for retrieving extinction and optical depth. To be consistent, the lidar ratio and multiple scattering function must be based on the same underlying aerosol or cloud particle model. A constant value for the lidar ratio, as well as an array (as a function of range) for the multiple scattering function, are specified for each feature for later use by the optical property retrieval.

If a feature is classified as stratospheric, on the other hand, no further typing is performed. Stratospheric classifications may be included in a future data release. The classification criteria used for features in the stratosphere will differ somewhat from those for features found in the troposphere, though the same general classification approach can be used (Table 6.4).

6.7   Aerosol Remote Sensing from POLDER

The retrieval method used for the retrieval of aerosol properties from POLDER (see Appendix A) data depends on the type of surface below the aerosol layer. We distinguish two cases: land and ocean surfaces. A comprehensive description of

Table 6.4 CALIOP science products and uncertainties

Data Product	Measurement Capabilities and Uncertainties
Aerosols	
Height, thickness	For layers with $\tau > 0.005$
τ, $\sigma(z)$	40%[a]
Clouds	
Height	For layers with $\tau > 0.01$
Thickness	For layers with $\tau < 5$
τ, $\sigma(z)$	Within a factor of 2 for $\tau < 5$
Ice/water phase	Layer by layer
Ice cloud emissivity, ε	± 0.05 for $\varepsilon > 0.1$
Ice particle size	$\pm 50\%$ for $\varepsilon > 0.2$

τ – optical depth
$\sigma(z)$ – profile of extinction cross-section
[a]assumes 30% uncertainty in backscatter-to-extinction ratio

aerosol retrieval from POLDER can be found at the ICARE web site (http://www-icare.univ-lille1.fr/parasol/?rubrique=overview_product).

6.7.1   POLDER Remote Sensing of Aerosols Over Ocean Surfaces

The method is based on a comparison between POLDER measurements and LUTs calculated for a set of aerosol models (size distribution, refractive index, optical thickness) for the POLDER observations. The inversion scheme mainly uses the normalized radiances in the 865 nm channel, where the ocean colour reflectance is zero, and in the 670 nm channel with a constant water reflectance of 0.001. The polarized Stokes parameters at 865 and 670 nm are also used to help to derive the best aerosol model.

The algorithm uses a bimodal aerosol model, which mixes a mode of small particles (S) and a mode of large particles (L) with respective optical thickness τ_S and τ_L, at 865 nm. A mode of small particles (S) consists of a lognormal size distribution of spherical particles with a given refractive index. A mode of large particles (L) consists of a mixture of spherical and non-spherical particles. The spherical particles are lognormally distributed and have a given refractive index. The non-spherical particles are described by the mean model given in Volten et al. (2001). The contributions of large spherical and non-spherical particles to the optical thickness at 865 nm are given by τ_{L-S} and τ_{L-NS}, respectively. The large modes are a combination between spherical large particles and non-spherical particles with a mixture concentration varying from 0 to 1 in steps of 0.25 (Herman et al. 2005). The set of the refractive indices and modal radii of the small and large spherical particles used depends on the viewing conditions. Given a small and a large mode of particles with a total optical thickness $\tau = \tau_S + \tau_L$, the corresponding radiance L is calculated using the approximation of Wang and Gordon (1994). A similar approach can be applied for the normalized Stokes parameters Q and U.

LUTs of the radiances (865, 670 and 565 nm channels) and of the Stokes parameters Q and U (865 nm, 670 nm and blue channels) are calculated for different small modes, large modes of spherical particles and one non-spherical mode, for 11 aerosol optical thicknesses from $\tau = 0$ (molecular case) to $\tau = 2.6$ (extreme turbid atmosphere). These calculations are made for 21 solar angles (3° to 77°), 20 viewing angles (3°–73°) and 37 relative azimuth angles from 0° to 180° (steps of 5°). Computations are performed with a rough ocean surface (Cox and Munk 1954) and a wind speed of 5 m/s. The foam contribution is calculated following Koepke (1984) and a constant value of 0.22 for the foam reflectance. When the aerosol content is low, we only consider a fixed aerosol model for which the aerosol optical thickness is deduced.

The retrieval algorithm follows a two-step procedure. First the concentration of the mode in terms of optical thickness and total optical thickness is adjusted to fit the total radiance for a given combination of the small and the large mode. Then the directional Stokes parameters L, Q and U are interpolated in the LUT in the 865 and 670 nm channels. The difference (rms) between these simulations and the measurements are computed for each couple of modes: the minimum value (best fit) gives the aerosol model (modes and the fine mode concentration) and the corresponding optical thickness at 865 nm.

6.7.2 POLDER Remote Sensing of Aerosols Over Land Surfaces

Aerosol remote sensing over land from visible radiance measurements is more difficult than over the ocean because the surface reflectance is generally much greater than that for aerosol, except over dark surfaces (vegetation in the blue channel, lakes in near infrared). Airborne experiments (Deuzé et al. 1993) have shown that the relative contribution of the surface compared to the atmosphere is less important in polarized light than in total light. The aerosol algorithm over land is based on a best fit between polarized POLDER measurements and data simulated for different atmospheres including several aerosol models for different optical thickness, and ground surfaces conditions. The surface contribution depends on the type of surface (Nadal and Bréon 1999). The surface polarized reflectance is multiplied by an exponential factor corresponding to the attenuation through the atmosphere. The atmospheric term contribution to the measured signal is interpolated in LUTs computed using a successive order of scattering code (Lenoble et al. 2007).

Over land, ground based measurements show that the aerosol polarization mainly comes from the small-spherical particles (Vermeulen et al. 2000) with radii less than about 0.5 μm corresponding to the accumulation mode. So, the aerosol models used in the algorithm consist of lognormal size distributions of spherical particles: their characteristics are close to those for the oceanic small mode.

Knowing the super-pixel characteristics (altitude, surface classification, normalized difference vegetation index, NDVI), the surface polarized radiances are computed in the 865 and 670 nm channels, for the given viewing directions. For a given

aerosol model, the aerosol optical thickness at 865 nm is adjusted with a root-mean square (rms) method to fit the polarized measurements. Then the rms are compared for the set of aerosol and the best solution corresponds to the minimum value, characterized by its Ångström exponent, and the associated optical thickness and a quality index indicating the confidence degree in the fit.

Fig. 6.2 shows examples of global monthly mean average aerosol products derived from POLDER, for May 2006.
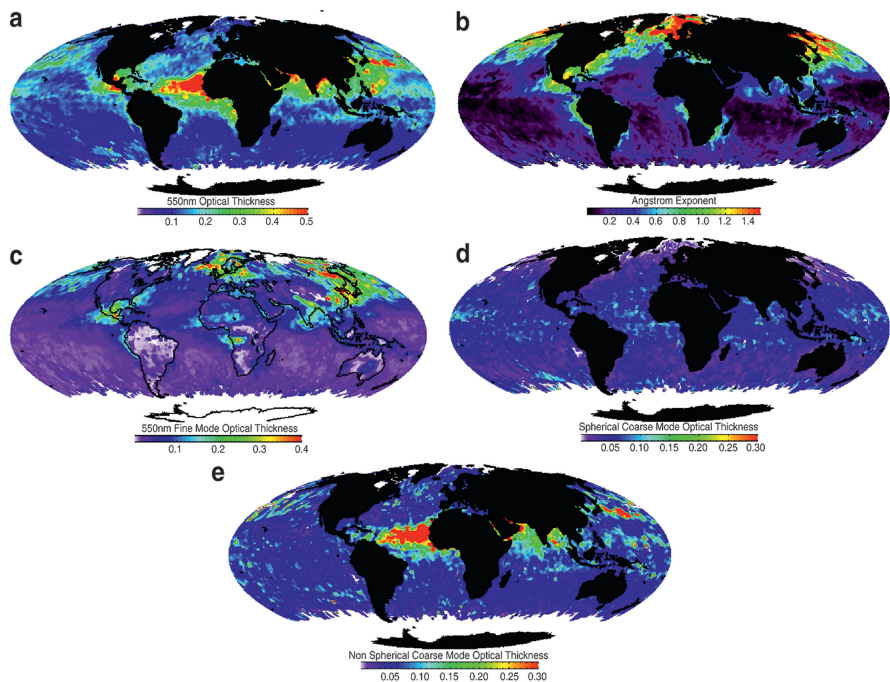
Fig. 6.2 Examples of aerosol information derived from POLDER for May 2006: (**a**) Total aerosol optical thickness; (**b**) Ångström exponent between 670 and 865 nm; (**c**) Fine mode aerosol optical thickness; (**d**) Spherical coarse mode aerosol; (**e**) Non spherical (dust) aerosol optical thickness (Credits: ICARE data center).

6.8 Retrieval of Aerosol Properties Using AATSR

The Advanced Along Track Scanning Radiometer (AATSR) on ENVISAT is the third in a series of ATSR instruments (see Section 6.1 and Appendix A). The data from these instruments have the potential of producing a 20 year aerosol record, starting in 1995. The AATSR dual view algorithm (ADV) has been used to provide aerosol data products over different areas such as the eastern part of the United States (Veefkind et al. 1998), Europe (Robles-Gonzalez et al. 2000; Veefkind et al. 2000), India and the Indian Ocean (Robles-Gonzalez et al. 2006)

and Africa (Robles-Gonzalez and de Leeuw 2008). A first step to develop products was made as part of the ESA Data Users Programme project TEMIS (Tropospheric Emission Monitoring Internet Service, www.temis.nl). Other efforts are underway as part of the Globaerosol project (ESA Date Users Element: http://dup.esrin.esa.it/projects/summaryp64.asp) where the algorithm used is that developed by the University of Oxford (Thomas et al. 2007). A third algorithm has been developed by the University of Swansea (Grey et al. 2006) which it is expected to apply to the production of global data sets. The algorithm discussed here (Veefkind et al. 1998; Veefkind and de Leeuw 1998), was developed at TNO (Netherlands Organisation for Applied Scientific Research) and transferred to the University of Helsinki and the Finnish Meteorological Institute (FMI) in 2007, where it is further developed and applied to provide aerosol data products for use in scientific studies.

6.8.1 AATSR Characteristics

AATSR is a dual view imaging spectrometer with seven wavelength bands, four in the visible and NIR (0.555, 0.659, 0.865, and 1.6 μm) and three in the mid- and thermal-infrared (3.7, 11, and 12 μm). The resolution of the instrument is $1 \times 1 \text{ km}^2$ at nadir view and the swath width is 512 km, resulting in a return time of approximately 3 days at mid-latitudes. AATSR has two cameras which provide a nadir view and a forward view at 55° incident angle to the surface. Together these two views allow for near-simultaneous observation of an area on the Earth's surface through two different atmospheric columns within a time interval of about 2 min.

AATSR was primarily designed for the measurement of water temperature but its characteristics render the instrument suitable for aerosol retrieval as well, in particular over land where the dual view is used to eliminate land surface effects on the radiation at the TOA (Veefkind et al. 1998). Over water a single view is used (Veefkind and de Leeuw 1998). Both algorithms include multiple scattering and the bi-directional reflectance of the surface. A drawback is the small swath of 512 km which results in a global coverage at the equator in approximately 5 days.

6.8.2 AATSR Retrieval Algorithm

The upwelling radiances measured at the top of the atmosphere in the visible and NIR channels are used for the retrieval of aerosol properties (AOD, the Ångström parameter and the mixing ratio of dominant aerosol classes). The 0.659 μm, 0.865 μm, and the 11 and 12 μm channels, are additionally used for cloud detection. When clouds are present, their radiance dominates the TOA signal and aerosol properties cannot be retrieved.

To discriminate between cloudy and cloud free areas over land, three tests are applied. These tests are based on the brightness temperature at 11 μm, the

reflectance at 0.659 μm and the ratio of the reflectance at 0.865 μm to the reflectance at 0.659 μm. The reflectance of clouds is similar in these channels, whereas over land, the surface reflectance at 0.865 μm is generally higher than at 0.659 μm. Hence, over clouds the ratio should be around 1 and larger over land. Over water the effect is the opposite: a reflectance ratio threshold lower than 1 indicates cloud free pixel over water (Robles Gonzalez 2003).

The core of the algorithm is the derivation of aerosol optical properties for cloud-free pixels, which is accomplished by comparing the measured TOA reflectance to reflectances calculated by a radiative transfer model and stored in LUTs. The difference between the modelled and measured TOA reflectances at each suitable wavelength (0.555 μm, 0.659 μm and 1.600 μm over land) is determined for a range of aerosol mixtures and the error function for all three wavelengths together is minimized to determine the best fit for both the AOD and the aerosol mixing ratio. The radiative transfer model used is DAK (Double Adding KNMI) (de Haan et al. 1987; Stammes 2001) developed at the Royal Netherlands Meteorological Institute (KNMI). A variety of aerosol models and mixtures of these are used as appropriate for the region of interest.

Over dark surfaces, such as over open ocean or dark vegetation, the AOD can be determined directly using a single view (Veefkind and de Leeuw 1998). Over brighter surfaces, the effects of the surface reflection and the atmospheric reflection on the TOA reflectance need to be separated. This is accomplished by taking advantage of the two views provided by AATSR as described in Veefkind et al. (1998).

In the dual-view algorithm, it is assumed that k, the ratio between the surface reflectances in the nadir and the forward views, is independent of the wavelength (Flowerdew and Haigh 1995). Hence k can be determined at 1.6 μm, where the effect of aerosol is minimal and is ignored in the first retrieval step to obtain a first estimate of the AOD. In the next iteration this AOD is used as a first guess and the parameters are adjusted.

6.8.3 AATSR Products

The retrieval is made for single pixels (1×1 km at nadir). Results are evaluated by comparison with AERONET Sun Photometer data. Post-processing includes re-gridding to 10×10 km^2. In the distribution of AOD values both the highest and the lowest outliers are removed. This procedure is based on the assumption that no large gradients are expected in the aerosol concentrations on a scale of 10 km, unless intensive point sources are present.

Products are the spectral AOD for 0.555 μm, 0.659 μm and 1.6 μm (and at 0.865 μm over water) and the Ångström coefficient. The aerosol mixing ratio, which is the optimum mixture of two aerosol types is, in principle, also available (Robles-Gonzalez et al. 2006; Robles-Gonzalez and de Leeuw 2008). As an example, we show results obtained during UAE2 (the United Arab Emirates Unified

Aerosol Experiment) over the United Arab Emirates and the Persian Gulf (Reid et al. 2005) in Fig. 6.3 (AOD) and the comparison of retrieved AOD with simultaneous AERONET data over water and over land in Fig. 6.4 (de Leeuw et al. 2005).
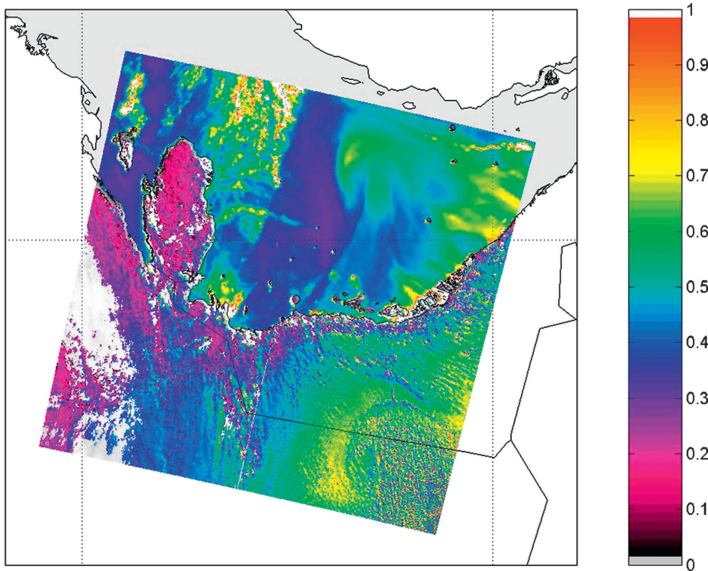
Fig. 6.3 AOD at 0.67 μm over the UAE area retrieved from AATSR data on 7th September 2004 (de Leeuw et al. 2005).
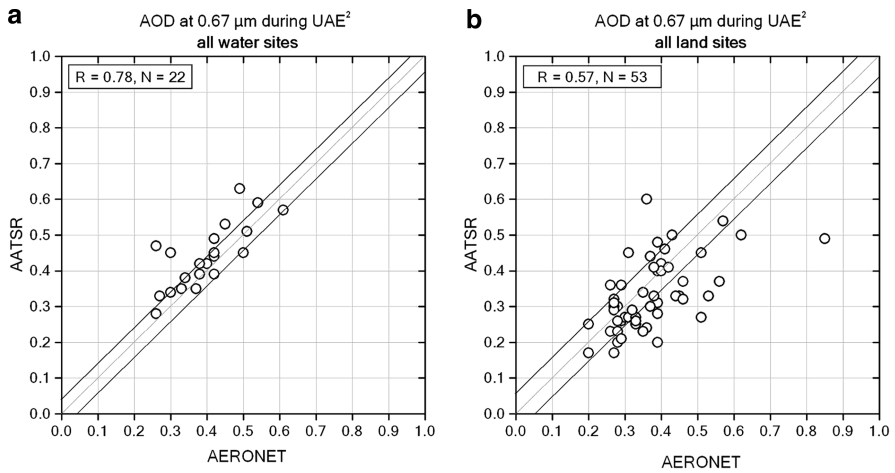
Fig. 6.4 Comparison of AOD derived from AATSR data during UAE2 with AERONET sun photometer data, for all water sites (**a**), and for all land sites (**b**) (de Leeuw et al. 2005).

6.9   Aerosol Remote Sensing from Aqua/MODIS

The first MODIS instrument was launched onboard the EOS-Terra satellite in December 1999 (see Appendix A). In May 2002, a second MODIS instrument was launched on board EOS-Aqua. The MODIS instruments measure sunlight reflected by the Earth's atmosphere and surface and emitted thermal radiation at 36 wavelengths. At least two observations for any place in Europe are obtained per day during daylight hours because the Terra and Aqua satellites cross Europe near 10:30 and 13:30 local solar time, respectively. There are two different algorithms to retrieve aerosol properties over land and over ocean. A comprehensive description of the MODIS aerosol retrieval algorithm can be found at the MODIS atmosphere group web site (http://modis-atmos.gsfc.nasa.gov/MOD04_L2/index.html). The MODIS aerosol products are from Collection 5.

6.9.1   MODIS Remote Sensing of Aerosols Over Ocean Surfaces

The first step in the Ocean Algorithm is to organize the reflectance from the six wavelengths used in the procedure (0.55 µm, 0.66 µm, 0.86 µm, 1.24 µm, 1.6 µm and 2.13 µm) into 10 km × 10 km boxes of 20 × 20 pixels at 500 m resolution. The Ocean algorithm requires all 400 pixels in the box to be identified as ocean pixels by the MYD35 mask, which helps minimize problems introduced by shallow water near the coasts. If any land is encountered, the entire box is left for the land algorithm. The major issue with the retrieval of aerosol over ocean is the contamination by bright targets, i.e. either clouds or specular reflection on the water surface. The specular reflection (glint) depends on the geometry of observation. The Ocean Algorithm is designed to retrieve AOT for glint angle only over the dark ocean, away from the glint, i.e. when the glint angle is over 40° and in cloud-free pixels. Moreover, the brightest and darkest 25% of the pixels (reflectance values at 0.87 µm) are discarded to prevent contamination by residual clouds and cloud shadows.

The MODIS aerosol retrieval algorithm is based on LUT inversion. The top-of-the atmosphere radiances for the aerosol channels are computed for several viewing geometries, aerosol optical thicknesses and types. Computations are performed for 15 zenith view angles (θ_v = 1.5° to 88 by steps of 6°), 15 azimuth angles (φ = 0°–180° by steps of 12°) and 7 solar zenith angles (θ_s = 1.5°, 12°, 24°, 36°, 48°, 54°, 60°, 66° and 72°). Several values of aerosol total loading are considered for each mode and described by the optical thickness at 0.55 µm. Extreme conditions included in the LUT are pure molecular atmosphere ($\tau = 0.0$) and very turbid atmosphere ($\tau = 2.0$). Three intermediate values are considered ($\tau = 0.2, 0.5, 1.0$), and a linear interpolation between these values is applied. To account for effects of different aerosol types on the radiance at the top of the atmosphere, they are assumed to be an external mixture for which the total radiance can be approximated by the weighted average of the radiances of each individual mode for the

same optical thickness (Wang and Gordon 1994). The set of aerosol models is composed of four small modes and five large modes. The goal is to retrieve the ratio η of the small mode optical thickness to the total optical thickness for the set of the small and large modes giving the best fit between observations and measurements. The aerosol optical thickness at 0.550 μm is derived as a by-product. The selection of the aerosol models is performed by minimizing the rms difference between observed and modeled radiances.

The MODIS algorithm is presented by Remer et al. (2005). The flowchart in Fig. 6.5 illustrates the retrieval of aerosol properties over ocean surface.

6.9.2   MODIS Remote Sensing of Aerosols Over Land

Like the ocean algorithm, the land algorithm for MODIS data is an inversion, but it takes only three *nearly* independent observations of spectral reflectance (0.47, 0.66 and 2.1 μm) to retrieve three *nearly* independent pieces of information. These include total AOT at 0.55 μm, fine (model) weighting at 0.55 μm, and the surface reflectance at 2.1 μm. Like the ocean algorithm, the land algorithm is based on an LUT approach, i.e. radiative transfer calculations are pre-computed for a set of aerosol and surface parameters and compared with the observed radiation field. The algorithm assumes that one fine-dominated aerosol model and one coarse domi-nated aerosol model (each may be comprised of multiple lognormal modes) can be combined with proper weightings to represent the ambient aerosol properties over the target. Spectral reflectance from the LUT is compared with MODIS-measured spectral reflectance to find the best match. This best fit is the solution to the inversion. The processing of radiances can be described by the flowchart in Fig. 6.6 (Remer et al. 2005).

For Collection 5, Levy et al. (2007b) have replaced the surface reflectance assumption, the aerosol models and the LUT. The algorithm performs a simulta-neous inversion of two visible (0.47 and 0.66 μm) and one shortwave infrared (2.12 μm) channel, making use of the coarse aerosol information content in the shortwave infrared.

Fig. 6.7 shows examples of global monthly means derived from Aqua/MODIS: AOD and fine mode ratio of the AOD, from Aqua/MODIS at 550 nm.

6.10   Aerosol Properties from OMI

OMI (Appendix A) is an imaging UV-vis solar backscatter spectrometer. It is a Dutch–Finnish instrument onboard the NASA satellite EOS-Aura that was launched in July 2004. Earth radiance spectra are measured simultaneously on a 2,600 km wide swath and global coverage is achieved on a daily basis. The nadir pixel size is
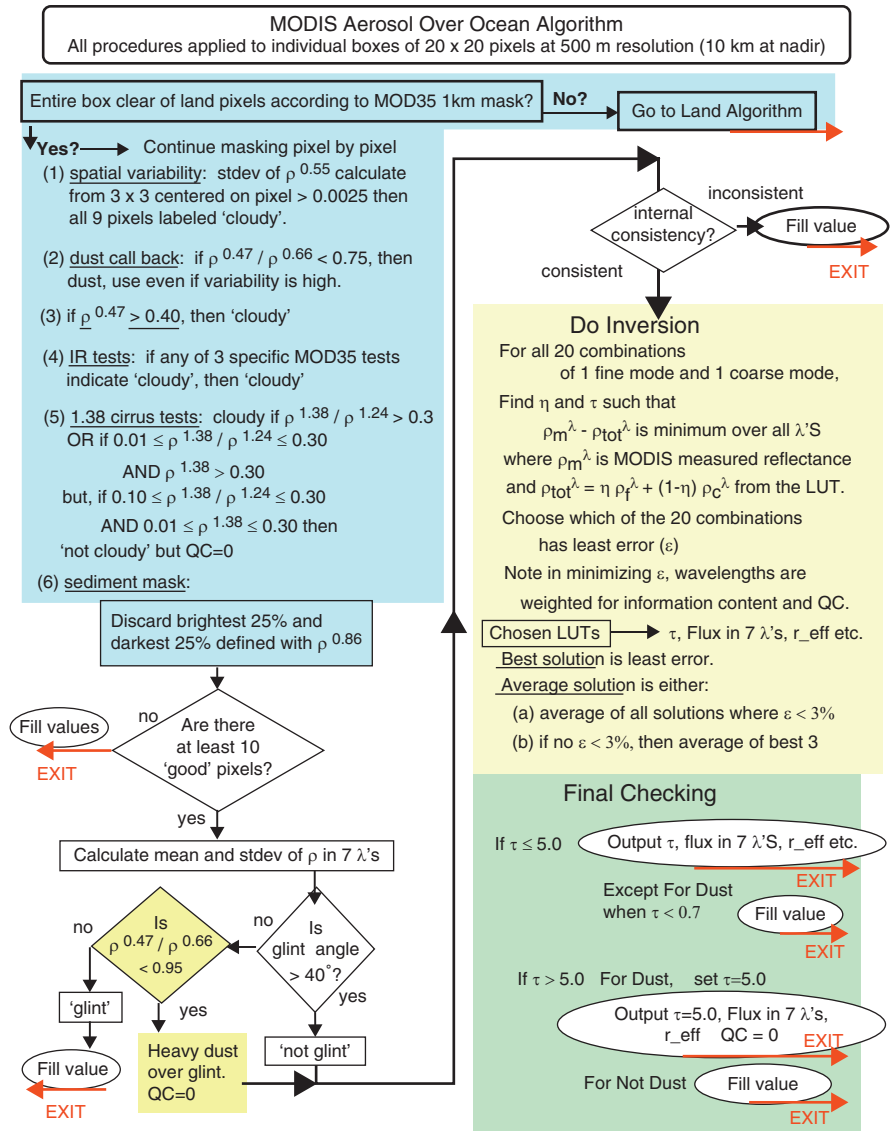
Fig. 6.5 Flowchart illustrating the retrieval of aerosol properties over ocean surfaces. Algorithm for remote sensing of tropospheric aerosol from MODIS Collection 5 (Remer et al. 2005).

13×24 km^2. Two aerosol products are derived from OMI measurements. The OMAERUV product (near-UV algorithm) is based on reflectance measurements at two wavelengths in the near-UV. It provides AOD and AAOD (Absorbing Aerosol Optical Depth) and the aerosol index. AAOD is sensitive to elevated absorbing

MODIS Over Land Algorithm
All procedures applied to individual boxes of 20 x 20 pixels at 500 m resolution (10 km at nadir)

- Ensure angles and reflectance values are valid. If not: report Fill values and EXIT
- Identify and mask (discard) all water, cloudy and snow/ice pixels.
- Identify "dark target pixels" that have $0.01 \leq \rho_{2.13} \leq 0.25$
- Discard brightest 50% and darkest 20% of pixels defined with $\rho_{0.66}$
  ... leaving a maximum of 120 pixels

Are there at least 12 (10%) dark target pixels?

yes — no

Procedure A
Set QA=0,1,2 or 3 (based on # of pixels)
- For all identified 'dark' pixels,
  Calculate mean $\rho_{0.47}$, $\rho_{0.66}$, $\rho_{2.1}$, $\rho_{1.2}$
  Calculate MVI = $MVI(\rho_{2.1}, \rho_{1.2})$
- Assume surface reflectance relationships:
  $\rho^{S}_{0.66} = f(\rho^{S}_{2.13}, MVI, \Theta)$ $\rho^{S}_{0.47} = f(\rho^{S}_{0.66})$
- Select fine model aerosol type LUT
  (function of geography and season)
- Select coarse model aerosol LUT (dust)
- Correct lookup tables for elevation
- Interpolate lookup tables on geometry

Do Inversion
For 13 values of η
  (-0.1,0.0,0.1,...0.9,1.0,1.1)...
Find $\tau_{0.55}$ and $\rho^{S}_{2.1}$ such that
  $\rho^{MODIS}_{0.47} - \rho^{TOA}_{0.47} = 0$,
where $\rho^{TOA}_{\lambda} = \eta(\rho^{fine}_{\lambda}) + (1-\eta)(\rho^{coarse}_{\lambda})$
Choose η such that
  $\rho^{MODIS}_{0.66} - \rho^{TOA}_{0.66} = \varepsilon$ is minimized
  Primary products: $\tau_{0.55}$, η, $\rho^{S}_{2.1}$, ε

- Calculate τ_{λ}, ρ^{S}_{λ}, α, MC, τ^{fine}_{λ}
- If $\eta = -0.1$ set $\eta = 0.0$; If $\eta = 1.1$ set $\eta = 1.0$
- If $\tau_{0.55} < 0.2$, then set η = Fill
- If $\varepsilon > 0.25$, then set QA = 0

Is $\tau_{0.55} < 0.0$?

Procedure B
Set QA=0
Identify and count pixels where
  $\rho_{2.13} > 0.25$ and $\rho_{2.13} \leq 0.25$ $f(\mu,\mu_o) < 0.40$

yes — Is N ≥ 12? — no — Report Fill values & error codes EXIT

- Assume surface reflectance relationships:
  $\rho^{S}_{0.66} = f(\rho^{S}_{2.13}, MVI, \Theta)$ $\rho^{S}_{0.47} = f(\rho^{S}_{0.66})$
- Assume Continental aerosol model (only)
- Correct lookup tables for elevation
- Interpolate lookup table on geometry

Do Single Channel Retrieval
Find $\tau_{0.55}$ and $\rho^{S}_{2.1}$ such that
  $\rho^{MODIS}_{0.47} - \rho^{TOA}_{0.47} = 0$,
where $\rho^{TOA}_{\lambda} = \rho^{Continental}_{\lambda}$
  Primary products: $\tau_{0.55}$, $\rho^{S}_{2.1}$

- Calculate $\tau_{0.47}$, MC
- Set η, $\tau_{0.66}$, $\tau_{2.1}$, α, τ^{fine}_{λ} = Fill

If $\tau_{0.55} \leq 0.0$ then set α= Fill , MC=0, τ^{fine}_{λ}=0
If $-0.10 < \tau_{0.55} \leq -0.05$, then set τ_{λ} = -0.05
If $\tau_{0.55} \leq -0.10$, then set τ_{λ}, α, MC, τ^{fine}_{λ}= Fill

yes — no

Report: τ_{λ}, ρ^{S}_{λ}, α, MC, τ^{fine}_{λ}, QA, etc EXIT

Fig. 6.6 Flowchart illustrating the retrieval of aerosol properties over land. Algorithm for remote sensing of tropospheric aerosol from MODIS Collection 5 (Remer et al. 2005).

aerosols and, in contrast to AOD, can be determined over bright surfaces and clouds. The OMAERO product (multi-wavelength algorithm) is based on measurements in the UV-VIS wavelength region and is explained in the following section.

Fig. 6.7 Global distributions of aerosol optical depth (**a**), and small mode fraction of the aerosol optical depth (**b**), retrieved from Aqua/MODIS data at 550 nm, aggregated for the month of June in 2008 (1 × 1 degree resolution, color scale between 0 and 1) Figure: produced with the Giovanni online data system, developed and maintained by the NASA GES DISC.

6.10.1   Properties from OMI Using the Multi-Wavelength Algorithm

A multi-wavelength aerosol algorithm (OMAERO product) has been developed at KNMI to retrieve aerosol properties from OMI spectral reflectance measurements in the UV-Vis wavelength region (Torres et al. 2007). The AOD is retrieved and

a best fitting aerosol type is determined. The single-scattering albedo, the layer height and the size distribution associated with the best fitting aerosol type are also provided. The multi-wavelength algorithm uses the reflectance spectrum in the near UV and the visible wavelength range.

A simulation study on the aerosol information content of OMI spectral reflectance measurements shows that OMI measurements contain two to four degrees of freedom of signal (Veihelmann et al. 2007). Including the near UV enhances the capability of the retrieval to distinguish between weakly absorbing and strongly absorbing aerosol types. Therefore, the OMAERO product can provide additional information about the aerosol type compared with other aerosol products from sensors that do not include the near UV, such as MODIS, MISR or POLDER.

The multi-wavelength algorithm uses a set of aerosol models, including models for desert dust, biomass burning, volcanic and weakly absorbing aerosol. All aerosol types are assumed to be spherical, except desert dust. The non-sphericity of desert dust is taken into account using the spheroidal shape approximation assuming the shape distribution that is used in AERONET retrievals for non-spherical aerosol types. Accounting for particle non-sphericity yields a significant improvement of the retrieved optical thickness when desert dust aerosol is present.

6.10.2 Status of the OMAERO Product

For ocean scenes, global AOD data from the OMAERO product have been compared with other products for June 2006. The comparison with quality assured data (MODIS QA flag = 3) from the MODIS standard product (Fig. 6.8, left) shows excellent agreement between the datasets. Note the use of this data flag excludes many scenes that were not flagged by the OMI cloud screening scheme. A comparison with POLDER data shows good agreement between the datasets (Fig. 6.8, right).
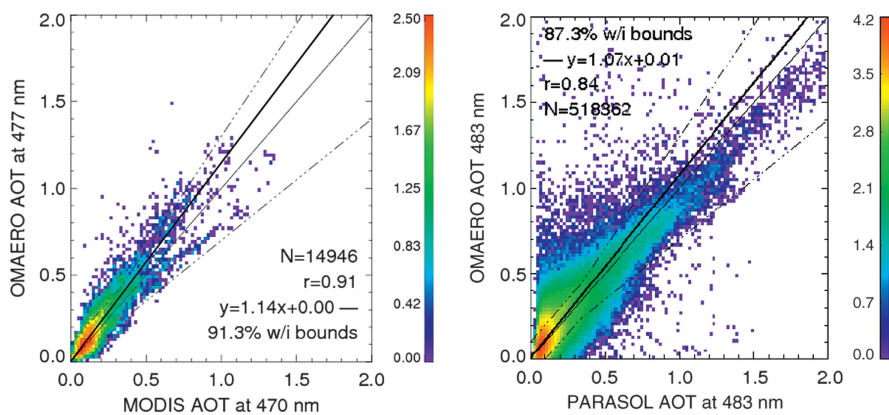
Fig. 6.8 AOD from the OMAERO product compared with quality assured data from the MODIS standard product (*left*) and with quality parameter filtered data from POLDER (*right*).

Curier et al. (2008) compared OMAERO and MODIS data over Europe and adjacent oceans and report correlation coefficients between 0.76 and 0.81 for scenes over ocean and between 0.59 and 0.70 for scenes over land. Current OMAERO data over land may be affected by errors in the surface albedo climatology. Reprocessing with an improved surface albedo climatology is envisaged. The main limitation of OMAERO aerosol data is cloud contamination. Cloud-contaminated scenes cannot be screened out without misclassifying scenes with large aerosol loadings as cloudy. The impact of cloud contamination is being investigated.

6.11   Retrieval of Aerosol Properties Using MERIS

MERIS (Appendix A) on ENVISAT is an instrument designed to measure ocean colour. Other MERIS products include atmospheric properties such as information about clouds and aerosols. The official ESA aerosol product uses the algorithm developed by Santer et al. (1999; 2000). The results have been evaluated by Höller et al. (2007). Non-operational scientific algorithms have been developed; an example is the Bremen AErosol Retrieval (BAER) algorithm discussed below.

In BAER (von Hoyningen-Huene et al. 2003; 2006), the Rayleigh path reflectance is calculated using a radiative transfer model, with the Rayleigh optical thickness for the required wavelengths (Buchholz 1995), the Rayleigh phase function, the illumination and viewing geometry and the actual temperature and pressure conditions at the surface. The barometric height equation and the dry adiabatic lapse rate are used, together with a digital elevation model (GTOPO30), to correct the Rayleigh path reflectance and air mass factors to the actual conditions within the satellite scene.

The correction for surface effects requires the application of a surface model, which can be adapted to the spectral and geometric conditions of the satellite scene. In BAER, a bi-directional reflection function (BRDF), normalized to the nadir position, is used that is based on the Raman-Pinty-Verstraete model (RPV) (Maignan et al 2004). The shape of the BRDF can be described by three parameters which depend on surface type. Currently BAER uses one set of BRDF parameters for the whole scene, ignoring regional variations.

The spectral properties and the magnitude of the surface reflectance are described by a bi-directional scattering distribution function, BSDF. Two basic spectra for "green vegetation" and "bare soil" are used, obtained from averages of the LACE-98 experiment, combined with measurement of the AVIRIS instrument to cover the whole spectral range. The green vegetation and bare soil spectra are linearly mixed, using the vegetation fraction taken from the atmospherically corrected NDVI of the scene, and a scaling factor is used to adapt the spectrum to the radiation conditions in the scene. An initial estimate for the aerosol reflectance is provided by assuming a "black" surface. The accurate estimation of the surface term by the spectral surface model is important, because a deviation of the surface reflectance of 0.01 leads to a change in AOD of about 0.1, depending on aerosol type.

The AOD retrieval is based on a LUT approach. LUTs are derived from radiative transfer modelling for a given BSDF, aerosol phase function, single scattering albedo, for AOD varying between 0 and 2.5, and Rayleigh scattering. The LUT is calculated for each of the MERIS wavelengths and for a range of viewing geometries. The phase function and single scattering albedo are obtained either using an aerosol data base like OPAC (Hess et al. 1998) or from the data base determined from AERONET sun-/sky radiometer measurements (Dubovik et al. 2000; 2002; 2006), or from campaigns such as ACE-2, LACE-98, SAMUM (von Hoyningen-Huene and Posse 1997; von Hoyningen-Huene et al. 1999a; 1999b; 2003; 2008; Silva et al. 2002).

The phase functions are normalized to 1 (in 1/sr). The spectral change in the phase function for wavelengths between 0.412 μm and 0.670 μm is neglected for retrieval over land, because, experimentally, no significant variation was observed. Also the spectral change in single scattering albedo is neglected because it is small within the spectral range. The set of selectable LUTs in BAER is presented in Table 6.5.

The results obtained with LUT No. 6, LACE-98, non-absorbing aerosol, compare well with AERONET AOD values. In cases with strong pollution high AOD tends to be underestimated by up to 20% with this LUT. In such cases a LUT with more absorbing aerosol needs to be selected.

The AOD is determined by minimizing the sum of the deviations between each of the individual estimates $\tau_{Aer}(\lambda_i)$ for channel i and the value $\overline{\tau_{Aer}}(\lambda_i)$ provided by the Ångström power law for the given aerosol type:

$$RMSD = \frac{1}{N} \sqrt{\Sigma_{i=1}^{N} \left(\tau_{Aer}(\lambda_i) - \overline{\tau_{Aer}}(\lambda_i) \right)^2} \qquad (6.13)$$

The minimization is achieved by modifying the surface reflectance in an iterative scheme running over k:

$$\rho_{Surf,k}(\lambda) = \rho_{Surf,k-1}(\lambda) \cdot w(\lambda) \cdot \left(1 - \frac{\tau_{Aer,k}(\lambda) - \overline{\tau_{Aer,k}}(\lambda)}{\tau_{Aer,k}(\lambda)}\right) \qquad (6.14)$$

until RMSD < 0.005 is reached.

The Ångström parameters are calculated by a least square fit of the retrieved AOD for all used spectral channels, i.e. channels 1–7 over land, instead of the commonly applied two-channel-approaches of Eck et al. (1999). The use of

Table 6.5 Look-up-tables in use and their characteristics

LUT number	Aerosol model	Phase function	Single scattering albedo
1	Clean marine	OPAC, clean marine	1.0
2	Clean continental	OPAC, clean continental	0.975
3	Average continental	OPAC, average continental	0.928
4	ACE-2, marine	ACE-2, experimental	1.0
5	LACE-98, absorbing	LACE-98, experimental	0.98
6	LACE-98, non-abs.	LACE-98, experimental	1.0
7	Desert	SAMUM, experimental	0.97

the Ångström power law ensures a sufficient smoothness of the AOD spectrum. In the first iteration the spectral slope α is determined from the retrieved value of the AOD. It is constrained to $-0.5 \leq \alpha \leq 2.0$. If the retrieved spectral slope is outside this limit, it is set to the climatological average of $\alpha = 1.3$

For the first iteration, the surface reflectance obtained from the BRDF data base is used to determine the AOD. Then the spectral surface reflectance is modified, Eq. 6.14, depending on deviations of the smoothed spectral AOD. Using the modified surface reflectance, an improved AOD is obtained. This procedure is repeated, until RMSD has reached its defined minimum. The retrieval uses 7 wavebands, with different weighing factors. The main steps of BAER described in the previous sections are summarized in Fig. 6.9.
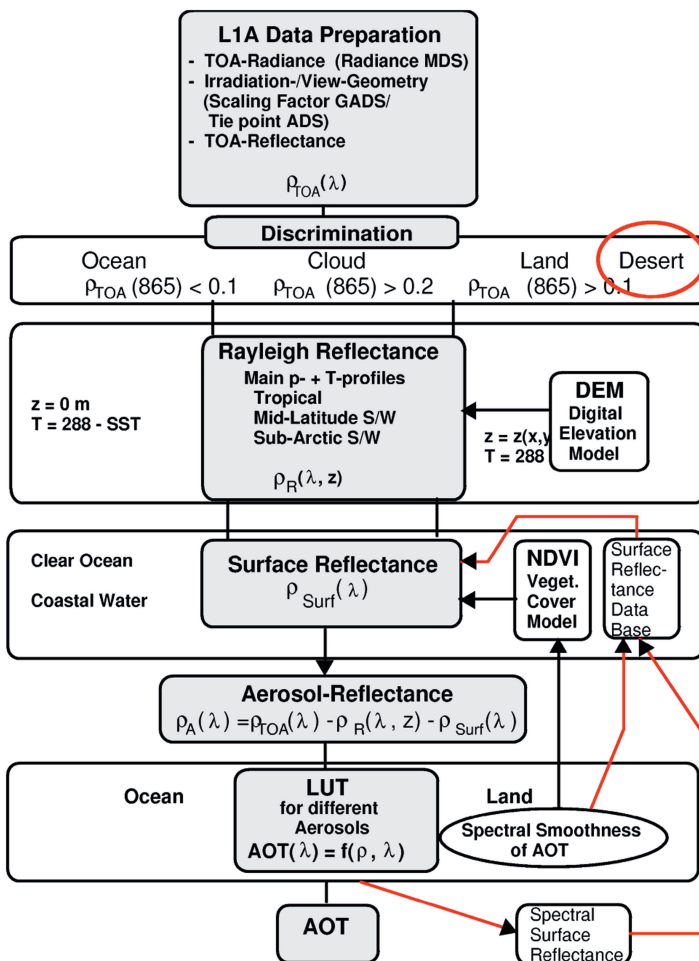
Fig. 6.9 A flow diagram for the BAER algorithm; Dinter et al. (2009).

6.12   Validation

The need for validation is discussed in Chapter 7. For algorithm development it is important to test different schemes using different approaches in order to deal with the surface reflectance, especially over land, and using different aerosol models. This is clearly illustrated by the upgrade of the MODIS algorithm used for Collection 5 (C005) processing where both these aspects were considerably revised. The validation of the treatment of the surface reflectance is a difficult issue and data on the surface reflectance from different instruments often are significantly different due to pixel size and measurement methodology. Usually only the end product can be evaluated, i.e. the AOD which is compared with ground-based measurements available from the AERONET sun photometer network (Holben et al. 1998) with some hundreds of stations over land having similar instruments (CIMEL sun photometers of different types), or lidar networks (see http://www.earlinet.org/) to obtain information on the vertical structure (see Chapter 7).

AERONET was extended with the maritime aerosol network (MAN) in 2008 (Smirnov et al. 2009). MAN utilizes hand held sun photometers (Microtops) which are deployed during research cruises over the world oceans. These are particularly important because they provide surface measurements over the open-ocean where no other data are available for validation and evaluation of satellite data. It is known that a variety of aerosol conditions may occur over the open ocean, for example the transport of dust, transport of biomass burning and pollutants, or a very clean maritime atmosphere with very low AOD close to the measurement uncertainty. Several other sun photometer networks are part of AERONET such as the European PHOTONS and the Canadian AEROCAN, and complimentary networks are maintained such as GAW-PFR (Global Atmosphere Watch – Precision Filter Radiometer) in remote locations. In addition there are a number of national networks making direct sun measurements.

Ground-based *in situ* measurements are performed at many sites world-wide, but they are poorly coordinated and with different procedures and protocols. The EU-funded EUSAAR project (European Supersites for Atmospheric Aerosol Research) aims at harmonizing 20 selected aerosol supersites in Europe measuring chemical, physical and optical properties, and making the data available through a specialized data center. Quality control is an important issue in EUSAAR.

6.13   Air Quality: Using AOD to Monitor PM2.5
in the Netherlands

Satellite measurements provide full spatial coverage of the Earth and are – in principle – consistent for the whole European region. So, although they are less precise than *in situ* observations, satellite measurements may be useful to improve the insight in regional PM distributions and so be complementary to ground-based

measurements. The key parameter to derive PM distributions from satellite data is the AOD. Empirical relations between AOD and PM10 or PM2.5 measurements have been reported for different parts of the world (Wang and Christopher 2003; Hutchison 2003; Engel-Cox et al. 2004; 2006; Al-Saadi et al. 2005; Schaap et al. 2008) (and references therein). For example, promising correlations have been found between time-series of AOD and PM2.5 for many stations in eastern and midwest U.S. Other stations, however, particularly in the western US, show hardly any correlation (Wang and Christopher 2003; Hutchison 2003; Engel-Cox et al. 2004). Variations in local meteorological conditions, occurrence of multiple aerosol layers, and variations in aerosol chemical composition are likely to play an important role in determining the strengths of such correlations. To acquire estimates of PM2.5 distributions, one depends critically on an established relation between AOD and ground level PM2.5.

As an example to illustrate the use of satellite data to determine the spatial distribution of PM2.5, a study is described which was aimed at determining an empirical relationship between AOD and PM2.5 for the Netherlands from experimental data, and to explore the ability of mapping PM2.5 over the Netherlands using satellite-retrieved AOD data. The satellite data used are from MODIS because data are available from both the Terra over-flight in the morning (10:30 local time) and the Aqua over-flight in the afternoon (13:30 local time). Thus more data are available than from other instruments with a single daily overpass while the two MODIS over-flights also cover part of the diurnal cycle. In principle any satellite AOD data set could be used as well to provide daily AOD/PM2.5 maps (Kacenelenbogen et al. 2006) using POLDER data.

A field study to establish an empirical PM2.5 – AOD Relationship

To address the relation between AOD and PM2.5, a study was set-up to monitor PM2.5 between 1st August 2006, and 31st May 2007, at the Cabauw experimental site for atmospheric research (CESAR) (51.97°N, 4.93°E). The AOD measurements at Cabauw are made using a CIMEL sun photometer following the AERONET protocol (Holben et al. 2001). Measurements are made every 15 min and transmitted to the AERONET data base in near-real time by satellite. Initial cloud clearing takes place in a first processing step to provide Level 1.5 AOD data which were used in this study. The Level 2 data (pre- and post-field calibration applied, automatically cloud cleared and manually inspected) are updated on an annual basis. Level 2 data were used in this study for a sensitivity analysis. As semi-volatile ammonium nitrate levels are high in the Netherlands (Schaap et al. 2002), PM2.5 was monitored using a Tapered Element Oscillating Microbalance with Filter Dynamics Measurement System (TEOM-FDMS) to avoid losses. In addition to these core instruments, the RIVM aerosol backscatter lidar (Apituley et al. 2000) was extensively used for cloud detection. Three algorithms were used to detect clouds, i.e. a threshold method, a detection method for strong modulations in the lidar signal (Pal et al. 1992) and a method based on retrieval of the backscatter profile from the lidar data (Klett 1985) and setting a threshold at the scattering level of clouds.

6.13.1 Establishing an AOD-PM2.5 Relationship

As a first assessment, all AOD data were plotted against the collocated PM2.5 data in a scatter diagram (Fig. 6.10). At first glance, there seems to be a large variability and no indication for a well defined relation between the variables. Cases were selected with AOD values lower than 1 and PM2.5 concentrations smaller than 100 μg/m^3; some of the points outside these limits are clear outliers. A fit through these data shows that only 13% of the variability in PM2.5 is explained by AOD. Fig. 6.11 shows the complete time series of AOD and PM2.5. PM2.5 is given as a grey line and the AOD data are superimposed as diamonds. The time series for August–September (upper panel) shows that during August the PM2.5 concentrations were relatively low while often AOD was high. The two data sets are virtually uncorrelated during August. This is in contrast to the situation in September and in the spring of 2007 when the AOD and PM2.5 data track each other very well (R^2 ~0.6). The later data illustrate the potential to define situations in which the AOD may be used to estimate PM2.5 levels. However, the statistical analysis presented above (Fig. 6.10) was hampered by the occurrence of cloud contaminated AOD data. The lidar-based cloud screening of the L1.5 data strongly improved the correlation as shown in Fig. 6.11. About 50% of the data points was rejected, possibly because of the occurrence of broken cloud conditions and/or the presence of optically thin high cirrus clouds. The stricter cloud screening substantially improves the correlation between the AOD and PM2.5, resulting in a correlation coefficient R^2 = 0.41.
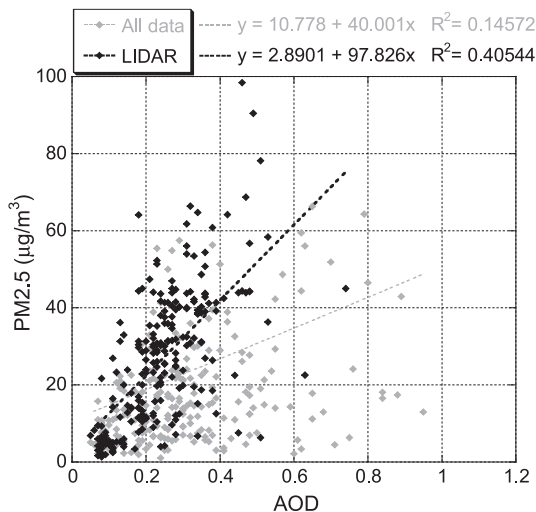
Fig. 6.10 Correlation between PM2.5 and sun photometer AOD at Cabauw before screening (*grey dots*) and after screening (*black dots*) for residual cloud contamination in the Aeronet AOD measurements.
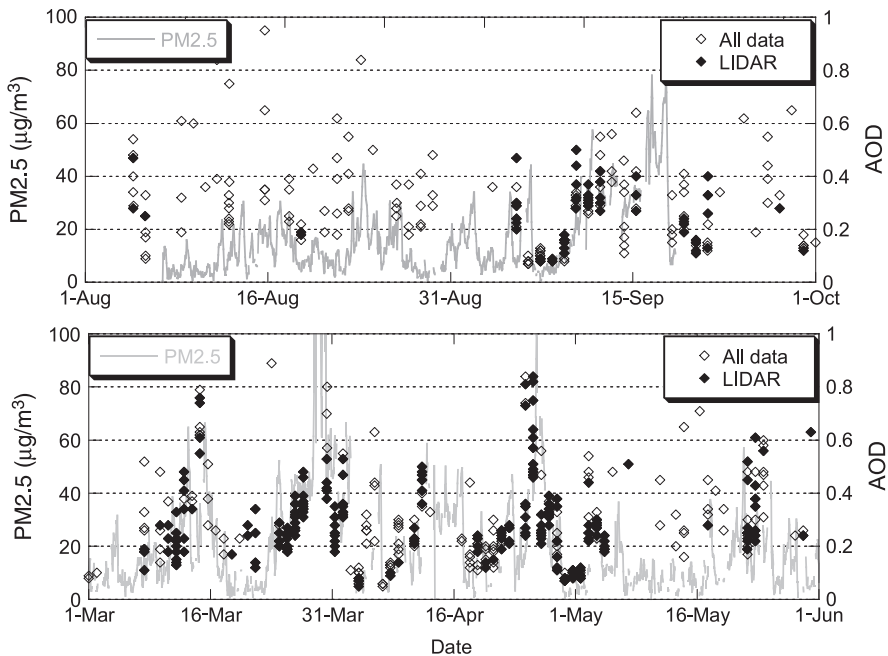
Fig. 6.11 Time series for PM2.5 and AOD for the period August–September (*upper panel*) and March–May (*lower panel*). The AERONET L1.5 AOD data are differentiated between data that did (*filled diamond*) and did not (*open diamonds*) pass our additional cloud screening.

It is noted that the problem of cloud contamination of the AERONET data does not occur when L2 data are used. However, L2 data are not available in NRT as are L1.5 data.

While the ground-based measurements of AOD and PM2.5 are obtained throughout the day, satellite observations of AOD provide "snap-shots" only during their overpass (typically once per day). In order to apply a relation between AOD and PM2.5 to AOD measurements from satellites, an investigation was made to determine whether the AOD-PM2.5 relation changes when the data was limited to the time window in which the MODIS instruments pass over Cabauw. MODIS/TERRA has their overpass in the late morning and MODIS/Aqua in the early afternoon. The effect of constraining the time window is illustrated in Fig. 6.12 for the period between 11:00 and 15:00 UTC. The overall reduction of available data points can be seen. Also, it was observed that a high percentage of the points on the edges of the data cloud are data points associated with early morning or late afternoon measurements. This is especially true for the points with low PM2.5 and moderately high AOD values. Strikingly, the explained variability increases when the time window is centered around midday. For that case, the following relationship between PM2.5 (in $\mu g/m^3$) and AOD was derived: PM2.5 $= 124.5$ AOD $- 0.34$ with $R^2 = 0.57$.

The relationship between AOD and PM observed at Cabauw may not apply to other areas, because of the spatial variation of aerosol sources and the subsequent
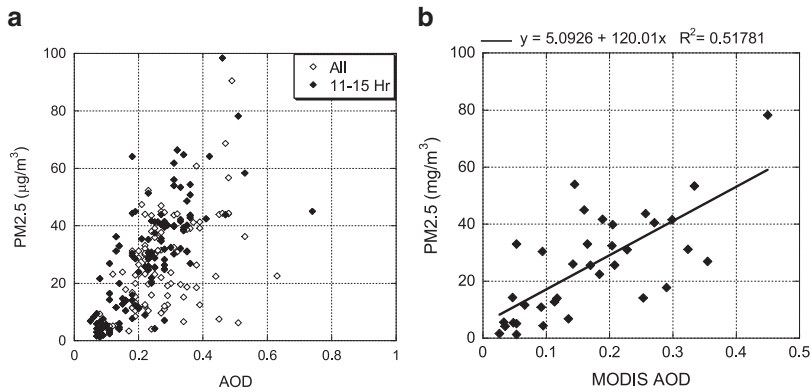
Fig. 6.12 (**a**) The variation of PM2.5 with AOD for all data and those between 11:00 and 15:00 h (Fit: PM2.5 = 124.5 AOD – 0.34); (**b**) The measured PM2.5 concentration as function of MODIS AOD. Note the difference in horizontal scales.

changes in aerosol properties due to chemical and physical processes which also affect the optical properties.

6.13.2 Application of the AOD-PM2.5 Relationship to MODIS Data

MODIS AOD was used to explore the application of the AOD-PM2.5 relation over the Netherlands. Figure 6.12b shows the variability of PM2.5 as function of MODIS AOD from the measurements at Cabauw, which is described by PM2.5 = 120 AOD + 5.1 $\mu g/m^3$. This fit explains 52% of the variability in PM2.5. The relation for the MODIS AOD is very similar to that determined with sun photometer data. It is noted that a systematic bias of 0.05 was identified in MODIS AOD compared to the sun photometer data, which explains the cut-off at 5.1 $\mu g/m^3$.

To derive a first estimate of the PM2.5 concentration field over the Netherlands based on MODIS data only, the AOD-PM2.5 relation was applied to the annual composite map of MODIS AOD. Results are presented in Fig. 6.13. High AOD values retrieved along the Dutch coast are likely to be an artifact. At land/water boundaries, application of the land algorithm to patches of sea often leads to high AOD values (Chu et al. 2002), while application of the ocean algorithm over coastal waters with suspended sediments (as in the North Sea) often gives rise to high AOD retrievals (Robles-Gonzalez et al. 2000; Chu et al. 2002; Ichoku et al. 2005). Hence, all pixels in which surface water covers more than 10% of the 10 × 10 km^2 grid were masked. Figure 6.13 shows that MODIS-AOD derived PM2.5 levels over the Netherlands are between 22 and 30 $\mu g/m^3$. The lowest PM2.5 concentrations, slightly over 11 $\mu g/m^3$, are mapped over the Ardennes and east of the Ruhr area. In the Ruhr area, the resulting PM2.5 levels are between 30 and 42 $\mu g/m^3$. Strikingly, the highest PM2.5 levels are mapped over south western Belgium and
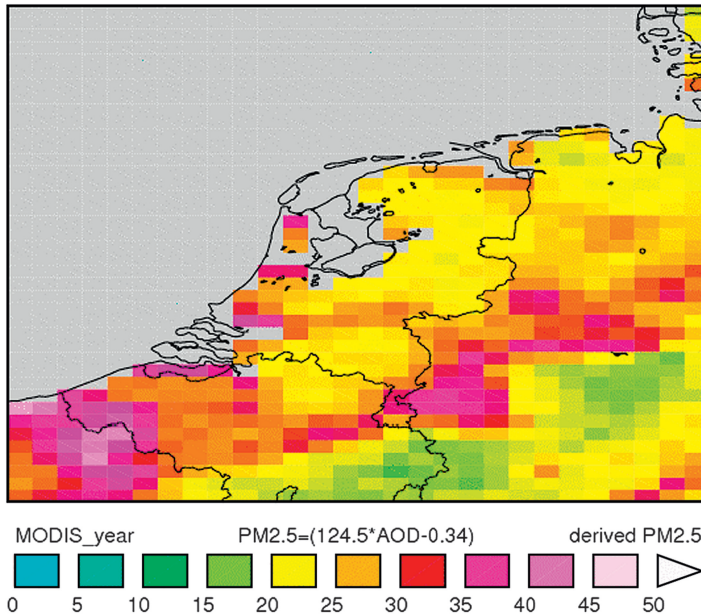
Fig. 6.13 Estimated PM2.5 distribution (μg/m^3) over the Netherlands and its direct surroundings, during situations with predominantly easterly and southerly flow, for which satellite retrievals are available.

northern France, in the region of Lille. Some features of the spatial distribution do not appear to be very realistic: the high values of PM2.5 around Lille and near the northern coast of the Netherlands for example. This might be caused by spatially varying systematic errors in the MODIS AOD data, which could be due to unaccounted variability in surface reflectance such as mixed land/water pixels. Because of the uncertainties in current satellite data of AOD, it is not expected that better PM2.5 maps can be constructed for the Netherlands based on satellite data alone without accounting for atmospheric processes. This conclusion may be specific for the Netherlands while other parts of continental Europe are less affected by the presence of mixed land/water pixels. Furthermore, the atmospheric boundary layer inland is often better mixed than near the coast, resulting in a more homogenous vertical distribution. Satellite measurements of AOD have added-value regarding the *temporal* variation of PM and can be useful in detecting trends and hot spots.

6.14 Application to Climate: Aerosol Direct Radiative Forcing

The aerosol direct effect is estimated in this work using off-line radiative transfer simulations. The necessary model input is based on global data-sets of monthly averages. In this particular approach, measurements and/or measurement-tied data, of sufficient accuracy, are preferred to model simulations. For aerosol, single scattering,

Table 6.6 Annual global averages for aerosol direct forcing

Aerosol forcing in W/m^2	Total (solar + IR)			Total (solar only)			Anthropogenic		
	Clr-sky	All-sky	Cld-eff	Clr-sky	All-sky	Cld-eff	Clr-sky	All-sky	Cld-eff
TOA	−2.7	−1.0	1.7	−3.8	−1.6	2.2	−0.7	−0.2	0.5
Atmosphere	3.4	3.7	0.3	4.3	4.2	−0.1	2.0	1.9	−0.1
Surface	−6.1	−4.7	1.4	−8.1	−5.8	2.3	−2.7	−2.1	0.6

column properties, monthly statistics at AERONET sites (Holben et al 1998) were merged into model median fields of advanced aerosol simulations in global modelling (Kinne et al. 2006). For the surface albedo characterization, MODIS (visible and near-IR land) data (Schaaf et al. 2002) were combined with SSM/I statistics (Basist et al. 1996) on ice and snow cover. Cloud data (required in all-sky simulations) are based on the ISCCP climatology (Rossow et al. 1993). The anthropogenic aerosol fraction (potential anthropogenic dust sources are ignored) and the aerosol vertical distribution are adopted from global modelling (Schulz et al. 2006). Simulated annual global averages for the aerosol direct effect and the aerosol direct anthropogenic forcing at the TOA, within the atmosphere and at the surface separately for cloud-free and all-sky conditions, are summarised in Table 6.6.

In the context of anthropogenic forcing to the entire Earth-Atmosphere-System the relevant aerosol value is defined by the anthropogenic TOA effect at all-sky conditions. Table 6.6 indicates a global annual average of −0.2 W/m^2 at the TOA level. This loss seems negligible, when compared to the 2.6 W/m^2 gain at the TOA level confidently attributed to enhanced greenhouse gas concentrations. Fig. 6.14 (annual map) and Fig. 6.15 (monthly maps) demonstrate, beyond global average values, that anthropogenic aerosol impact displays significant regional diversity. Largely, for a northern hemispheric impact, there are regions with strong cooling (e.g. industrial regions, oceans) or with strong warming (associated with advected pollution over highly reflecting surfaces such as deserts, snow and lower clouds).
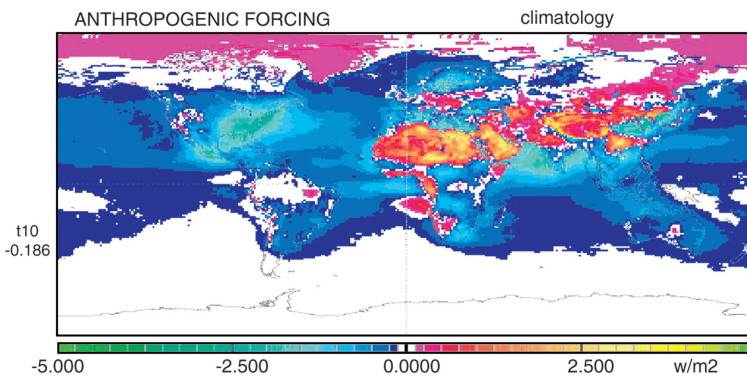
Fig. 6.14 Simulated annual anthropogenic aerosol direct (TOA) forcing at all-sky conditions based on monthly average input data-fields at 1 × 1 degree lat/lon resolution. Aerosol properties (AOD, ω$_o$ and g (via Ångström)) are tied to AERONET data, sub-spectral surface albedo data are based MODIS, ice and snow cover are obtained from SSM/I data and clouds are prescribed by ISCCP.

The strongest aerosol cooling occurs during the summer months in the northern hemisphere, when solar irradiance is at a maximum and snow cover at a minimum.

The inhomogeneity in Fig. 6.14 and Fig. 6.15 reflects the variability for aerosol and environmental input-fields. Despite a multi-annual data approach and the use of model-median data, the assumed monthly input data fields may contain significant errors, which would affect the overall result. Sensitivity tests were conducted, so that assumptions to individual input parameters could be modified.

jan
-0.132

may
-0.239

sep
-0.306

feb
-0.115

jun
-0.354

oct
-0.244

mar
-0.010

jul
-0.249

nov
-0.196

apr
-0.078

aug
-0.234

dec
-0.127

-9.000   -3.000   3.000   9.000   w/m2
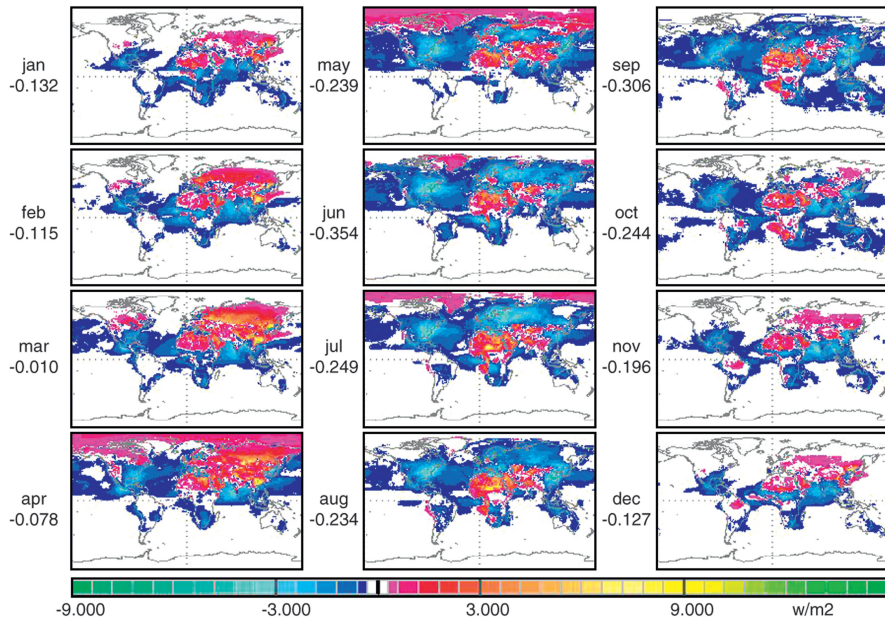
Fig. 6.15 Anthropogenic aerosol direct forcing of Fig. 6.14 at monthly resolution.

6.14.1   *Uncertainties in Aerosol Direct Radiative Forcing*

Sensitivity studies with modified input data indicate that, in the context of overall aerosol forcing uncertainty, and give the following results.

- The more consistent use of sky-photometer AERONET data for all aerosol properties over the favoured combination of sun and sky-photometer AERONET data (for better coverage and statistics on AOD and Ångström data) has only a small impact (estimated forcing uncertainty -0.01 to $+0.03$ W/m^2 globally). The uncertainty estimates reflect AERONET dataset differences on forcing.
- By using a different Ångström parameter threshold above which all AOD is assigned to the fine mode (here 1.8 instead of 2.1), the fine-mode probability is increased, yielding a 10% larger anthropogenic AOD (estimated forcing uncertainty -0.05 to $+0.01$ W/m^2 globally). The uncertainty estimate takes into account that the reference case assumes a relatively high Ångström threshold.

- A 25% increase in aerosol absorption reduces solar radiation losses to space and results in a significant reduction to aerosol cooling (+0.18 W/m^2 globally). Conversely, a 25% absorption decrease will increase aerosol cooling by a similar amount (estimated forcing uncertainty −0.07 to +0.07 W/m^2 globally). The uncertainty estimate considers that aerosol absorption is known within 10%.
- A 0.05 increase to the solar asymmetry-factor enhances the associated solar backscatter potential of aerosol which results in a reduction to aerosol cooling (+0.10 W/m^2 globally). Conversely, −0.05 decrease of the asymmetry-factor will increase aerosol cooling by a similar amount (estimated forcing uncertainty −0.07 to +0.07 W/m^2 globally). The uncertainty assumes asymmetry-factors to be accurate within 0.03.
- A 5% increase in land albedo strongly decreases the potential of aerosol to cool (+0.22 W/m^2 globally). Conversely, a 5% land albedo decrease will increase aerosol cooling by a similar amount (estimated forcing uncertainty −0.07 to +0.02 W/m^2 globally). The uncertainty estimate assumes the land-albedo on average to be accurate within 1% and the assumed MODIS-SSM/I solar albedo data produces slightly less cooling than with the use of IPCC median solar surface albedo fields.
- A lifting of the all aerosol by 2 km would allow for more "warming" contributions through an increased probability of (absorbing) aerosol above lower lying clouds results in an expected cooling reduction (+0.20 W/m^2 globally) (estimated forcing uncertainty −0.05 to +0.05 W/m^2 globally). The uncertainty estimate assumes that the relative placement between aerosol and clouds to be accurate within 0.5 km.

By combining all individual uncertainties and reducing the sum by 75%, because not all uncertainties are independent, for example, more absorption is associated with lower asymmetry-factors of smaller sizes, a probable range for the global annual aerosol direct forcing is estimated to fall between −0.45 and +0.00 W/m^2 with a high probability of the the most likely value near −0.2 W/m^2.

6.14.2   Comparisons of Aerosol Radiative Forcing with Models

The global annual average near −0.2 W/m^2 agrees well with the average of nine global models participating in the AeroCom forcing exercise (Schulz et al. 2006). The model averages, however, are lacking in regional contrast and in particular the strong warming over desert regions is missing. In that context, it cannot be ruled out that the applied MODIS data, in our hybrid approach, overestimate the surface albedo, especially in the near-infrared spectral region. In that case the most likely value could increase to about −0.25 W/m^2. In contrast, published results of other data-tied methods suggest a significantly more negative aerosol direct forcing of −0.9 W/m^2 (Quaas et al. 2008) or −0.8 W/m^2 (Bellouin et al. 2005). At closer inspection, it became apparent that poor assumptions caused negative biases, such

as ignoring snow cover and overestimating anthropogenic AOD in the Bellouin study, or neglecting aerosol above clouds and avoiding desert region in the Quaas study. Once properly corrected, almost all data-tied estimates fall within the expected range (0.45–0.0 W/m^2). Critical issues in data-tied aerosol direct forcing estimates are (1) the definition for aerosol anthropogenic fraction, (2) the aerosol impact in an all-sky environment, for example, absorbing aerosol above lower clouds "warms", (3) the frequent lack of global coverage, and (4) an incorrect representation of the solar surface albedo.

6.14.3 Aerosol Radiative Forcing: Conclusions

The global annual (anthropogenic) aerosol direct radiative forcing is estimated to be near -0.2 W/m^2. From expected uncertainties to aerosol and environmental properties, a likely range (-0.45 to 0.0W/m^2) was derived. This estimate is better than many data tied approaches, suggesting a stronger cooling, because they are biased towards more negative values by poor assumptions or poor data, which lead to too negative estimates for the direct aerosol effect in IPCC-4AR (-1.0 to -0.1 W/m^2 range). The simulated global annual average is in line with estimates from simulations with advanced aerosol modules in global models, but significant differences in the forcing patterns on a regional and seasonal basis need to be resolved. Major uncertainties in simulations of the aerosol direct forcing are the representation of surface albedo properties and also the representation of aerosol properties. With respect to the aerosol properties, comparisons with AERONET data suggest that modelling principally lacks fine mode absorbing aerosol. Larger uncertainties in aerosol direct forcing are associated with the aerosol characterization of absorption and size emphasising a need for regional quality data.

6.15 Use of Satellites for Aerosol-Cloud Interaction Studies

Satellite aerosol products can be used to support the evaluation of impacts of aerosol-cloud interactions on clouds. The relevant aerosol properties are listed below.

- Aerosol optical depth of the fine and coarse modes, which are proxies for small and large CCN, respectively.
- Aerosol absorption, which is relevant to the radiative impacts of the aerosols on clouds, by both "cloud burning" and blocking the surface solar heating.
- Aerosol sphericity, which is an indication of desert dust. Desert dust aerosols typically have relatively small CCN efficiency and high activity as ice nuclei.
- Aerosol index of refraction. This can be useful for restricting the aerosol composition, and/or assessing the amount of water absorbed by the hygroscopic

components of the aerosols. This is important for identification of increase of AOD due to absorption of water and growth into haze particles.

- Vertical distribution of the aerosols. This is important for determining whether the aerosols occur at the same height of the clouds, which is essential for their microphysical interactions.

This discussion shows the wide range of satellite applications and the required resolutions on spatial, vertical and temporal scales. The present satellites represent a trade-off between large coverage in space and time versus high quality data in much smaller domains. Of the parameters listed above, only the spectral AOD is available from most satellite instruments. The data products from several instruments are evaluated below, with an emphasis on the wish list presented above, and for products that are routinely available.

a   SEVIRI

The geostationary satellite, SEVIRI, provides imagery for the full disk every 15 min, but its shortest wavelength is 0.6 µm, which restricts the sensitivity to ultra fine aerosols that provide most of the CCN concentrations. The lack of mid-IR channels (2.1 µm) further restricts the usefulness of the MSG aerosols retrievals over land. The MSG has good sensitivity to the large desert dust aerosols, also during night-time due to their emissivity signature that is captured well by the 8.7, 10.8 and 12.0 µm channels of the MSG.

b   PARASOL

The POLDER/PARASOL instrument concept allows measurements of the spectral, directional and polarized light reflected by the Earth-Atmosphere system. Over land, where the surface contribution to the total radiance is generally large, the inversion scheme uses the polarized radiances in the 865, 670 nm and blue channels. As the largest particles (radius > 0.5 µm) generate low polarization, only the optical characteristics of the accumulation mode are derived. Over ocean, the characteristics of both aerosol modes (accumulation and coarse) are derived.

POLDER/PARASOL Aerosols products include the following parameters:

- Aerosol Optical Thickness (AOD),
- Ångström coefficient,
- Non-Sphericity Index for the Coarse Mode.

However, inspection of the products shows very sparse coverage and inconsistencies upon transition from land to ocean.

c   MODIS

MODIS aerosols are obtained from the polar Terra and Aqua polar orbiting satellites, approximately once a day. The MODIS aerosol products provide AOD

over land and ocean with a similar accuracy, except over the bright desert and ice covered areas. MODIS can separate the fine and coarse AOD over ocean, but less accurately over land due to poorer knowledge of the land surface spectral reflectance. The AOD over land for non-polluted situations occasionally provides negative AOD. This underlines the fact that MODIS AOD is not a good proxy for concentrations of small CCN, especially in such conditions.

d   OMI

OMI provides UV-Vis measurements with global coverage once per day. The OMAERUV product provides AOD and AAOD. The aerosol index allows the detection of elevated absorbing aerosols also over bright surfaces even over clouds. The OMAERO product provides the AOD and also the single-scattering albedo associated with the best fitting model. Reasonable sensitivity to small aerosols is achieved, although sensitivity is still lost below about 0.1 μm, which is the size that is most important for CCN activity. A limiting factor on the accuracy of the products is the large footprint (13×24 km^2 at nadir), which incurs an appreciable problem of cloud contamination. The influence of absorption by aerosols on the reflectance at the top of the atmosphere is enhanced in the UV as compared to longer wavelengths. Therefore OMI measurements provide complementary information on aerosol absorption when compared with other instruments that do not include the UV.

e   CALIPSO

CALIPSO, the space borne lidar, is unique in providing vertical profiles of aerosols, but only at the nadir pixel of the polar orbiting satellite. In addition to vertical profiles, CALIOP can retrieve aerosols in places where other sensors can't – over deserts, ice and snow, and above clouds. Aerosol forcing calculations presented in this chapter use model results for the aerosol profile, but there is a wide diversity in aerosol vertical distribution between different global models. CALIPSO data will be used to evaluate and improve the aerosol profiles predicted by models. Chand et al. (2009) show how CALIPSO data can be used to estimate the radiative forcing of aerosol above cloud and the necessity of considering instantaneous cloud fraction and cloud albedo along with the aerosol properties.

OMI, MODIS, POLDER and CALIPSO are all part of the A-Train and it is best to use them in combination.

6.16   Intercomparison of Aerosol Retrieval Products

Liu and Mishchenko (2008) compared AOD and Ångström parameters retrieved using TOA radiances measured with MISR and MODIS, two instruments that are dedicated to this purpose. They concluded that their analysis cannot be used to

determine which algorithm yields a more accurate retrieval in each particular case or which algorithm is better in general. Results from a comparison of MISR and MODIS aerosol products by Kahn et al. (2009) show good correlations between the AOD products (correlation coefficient 0.9 over ocean and 0.7 over land) and the Ångström exponent (correlation coefficient 0.67 over ocean when MISR AOD values > 0.2 are considered). Kahn et al. emphasize the necessity for the proper interpretation of the satellite products. In particular data-quality statements should be followed to ensure proper interpretation and use of the satellite aerosol products. Also other intercomparisons of satellite products reveal significant discrepancies between AOD (order of 0.1) from different instruments, even over ocean where aerosol retrieval should be easiest by virtue of the "dark" surface (Myhre et al. 2004; 2005). A recent comparison over land for a single scene (Kokhanovsky et al. 2007) shows that, even on the scale of a single pixel, there can be large differences in AOD retrieved over land using different retrieval techniques and instruments. However, these differences are not as pronounced for the average AOD over land. For instance, the average AOD at 0.55 μm for the area 7°–12°E, 49°–53°N was equal to 0.14 for MISR, NASA MODIS and POLDER algorithms. It is smaller by 0.01 for the ESA MERIS aerosol product and larger by 0.04 for the MERIS BAER algorithm. AOD derived using AATSR gives on average larger values as compared to all other instruments, while SCIAMACHY retrievals underestimate the aerosol loading. In a second paper, focusing on the AATSR Dual View (ADV) algorithm described in Section 6.8, Kokhanovsky et al. (2009) conclude that the results from the AATSR dual view algorithm compare favourably with the products from orbiting optical instruments dedicated for aerosol retrieval such as MODIS and MISR, which leads to the conclusion that AATSR is well suited for aerosol retrieval over land when the dual view is used together with the ATSR-DV algorithm.

6.17   Conclusions

The use of satellite products has substantially increased over the last decade as a source of data, complimentary to *in situ* measurements and model results, in support of studies on climate, climate change and air quality. Aerosol properties retrieved from satellite instruments provide spatial information on regional to global scales, obtained with the same instrument and the same assumptions and are thus, in this respect, consistent. Based on validation and intercomparison exercises, the uncertainty in the results can be determined. It is emphasized that satellite and *in situ* data are complimentary. Satellite data need to be validated and evaluated versus *in situ* data to understand both their strengths and their limitations. Regular validation is particularly important in order to recognize instrument drift and degradation. One of the strongest merits of satellites is that they provide continuous data with good spatial resolution over areas which are not, or not well, covered by ground-based observations.

An example demonstrating the application in air quality studies was presented in Section 6.13, and an example on the evaluation of the direct radiative effect of aerosols was presented in Section 6.14. In the latter study, sun-photometer data were used as a source for AOD. As an alternative, with better spatial coverage and at the expense of accuracy, satellite data can be used. Kinne (2009b) shows an example on the use of both sun photometer data form AERONET and satellite data from various instruments to provide global AOD maps. The use of satellite data for aerosol-cloud interaction studies is emerging and a preliminary evaluation of satellite products was presented in Section 6.15.

There is an increased demand for satellite aerosol products for model evaluation and AQ assessment. They are also used in scientific studies such as long range transport during Lagrangian experiments and to support observations in, for example, developing countries where satellite data providing spatial coverage are complementary to *in situ* point measurements.

The quality of the aerosol retrieval results varies between different instruments and different retrieval algorithms. Recent comparison exercises are given in Kokhanovsky et al. (2007; 2009). It is particularly important for the correct use of satellite products to consider the proper quality statements when these are available to avoid misinterpretation (Kahn et al. 2009). The use of products with low quality is generally not recommended.

Intercomparison between satellite data shows that no instrument can be singled out as providing the "best" data set. Aerosol retrieval from satellites is still a young science in full development. As discussed above, most instruments used for this purpose were designed with other applications in mind but turn out to provide useful information on aerosol properties. Few dedicated instruments have been launched and the full potential is still being explored. Apart from AOD and derived aerosol properties, aerosol layer height detection using stereo techniques is explored for the detection of aerosol plume properties, in particular for forest fires plumes (Kahn et al. 2007), which require multiple views.

Trends are the synergistic use of different instruments, preferably flying on the same platform. One such approach is the combination of a radiometer and a spectrometer in the SYNAER algorithm (Holzer-Popp et al. 2002). The current version of SYNAER uses AATSR to determine the surface reflectance and the spectral information from SCIAMACHY to retrieve aerosol type information. More recent approaches aim at using the different views provided by AATSR and MERIS to determine aerosol information over ocean (Sogacheva et al. 2009) and over land (North et al. 2008). These initiatives are of particular importance because of the continuation of very similar instrument deployments during future missions such as the sentinels which are prepared by ESA and EUMETSAT.

The GLORY mission (Mishchenko et al. 2007), briefly discussed in Section 6.5, will combine polarimetric measurements with multi-angle viewing, i.e. the instrument characteristics needed to obtain optimum information on aerosol properties. One of the primary objectives of the GLORY mission is to determine the global distribution of aerosol and cloud properties with very high accuracy, and thereby

facilitate the quantification of the aerosol direct and indirect effects on climate (Mishchenko et al. 2007).

Efforts to provide dedicated instruments and the exploration of synergies between different instruments will further improve the accuracy and consistency of data products. The expectation is that the use of satellite-retrieved aerosol properties for climate and air quality assessment will continue to increase and contribute to a better understanding of climate change leading to a reduction in the uncertainties. Satellite observations will play a larger role in air quality monitoring and the quantification of the aerosol emissions and their precursor gases.

References

Al-Saadi, J., J. Szykman, R.B. Pierce, C. Kittaka, D. Neil, D.A. Chu, L. Remer, L. Gumley, E. Prins, L. Weinstock, C. MacDonald, R. Wayland, F. Dimmick and J. Fishman, 2005, Improving national air quality forecasts with satellite aerosol observations. Bulletin of the American Meteorological Society, **86**, 1249–1261.

Ackerman, S.A., K.I. Strabala, W.P. Menzel, R.A. Frey, C.C. Moeller, and L.E. Guclusteringey, 1998, Discriminating clear sky from clouds with MODIS. J. Geophys. Res., **103**, 141−157.

Andreae, M.O., and D. Rosenfeld, 2008, Aerosol-cloud-precipitation interactions. Part 1. The nature and sources of could-active aerosols. Earth-Sci Rev, **89**, 13–41.

Apituley, A., A. Van Lammeren and H. Russchenberg, 2000, High time resolution cloud measurements with lidar during CLARA. Phys. Chem. Ear., **25**, 107–113.

Basist, A., D. Garrett, R. Ferraro, N.C. Grody, and K. Mitchell, 1996, A comparison between visible and Microwave snow cover products derived from satellite observations. J. Appl. Meteor., **35**, 163–177.

Bellouin, N., O. Boucher, J. Hayward and M. Reddy, 2005, Global estimate of aerosol direct radiative forcing from satellite measurements, Nature, **438**, 1138–1141.

Buchholz, A., 1995, Rayleigh scattering calculations for the terrestrial atmosphere. Applied Optics **34**, 2765–2773.

Cairns, B., F. Waquet, K. Knobelspiesse, J. Chowdhary and J.-L Deuzé, 2009, Polarimetric remote sensing of aerosols over land surfaces, In: A.A. Kokhanovsky and G. de Leeuw (editors) Satellite Aerosol Remote Sensing Over Land, Springer, Berlin, 295–323.

Chand, D., R. Wood, T.L. Anderson, S.K. Satheesh, and R.J. Charlson, 2009, Satellite-derived direct radiative effect of aerosols dependent on cloud cover, Nature Geoscience, **2**, 181–184, doi:10.1038/NGE0437.

Chu, D.A., Y.J. Kaufman, C. Ichoku, L.A. Remer, D. Tanré, B.N. Holben, 2002, Validation of MODIS aerosol optical thickness retrieval over land. Geophys. Res. Lett., **29**, doi:10.1029/2001GL013205.

Cox, C., and W. Munk, 1954, Measurements of the roughness of the sea surface from photographs of the Sun's glitter. J. Opt. Soc. Am., **44**, 838–850.

Curier R.L., J.P. Veefkind, R. Braak, B. Veihelmann, O. Torres and G. de Leeuw, 2008, Retrieval of aerosol optical properties from OMI radiances using a multiwavelength algorithm: Application to western Europe. J. Geophys. Res., 113, D17S90, doi:10.1029/2007JD008738.

de Haan J.F., P.B. Bosma, and J.W. Hovenier, 1987, The adding method for multiple scattering calculations of polarized light. Astron. Astrophys., 183, 371–391.

de Leeuw, G., and A. Kokhanovsky, 2009, Introduction, In: A.A. Kokhanovsky and G. de Leeuw (editors) Satellite Aerosol Remote Sensing Over Land, Springer, Berlin, 1–18.

de Leeuw, G., A.N. de Jong, J. Kusmierczyk-Michulec, R. Schoemaker, M. Moerman, P. Fritz, J. Reid and B. Holben, 2005, Aerosol Retrieval Using Transmission and Multispectral AATSR Data, in: J.S. Reid, S.J. Piketh, R. Kahn, R.T. Bruintjes and B.N. Holben (editors) A Summary of First Year Activities of the United Arab Emirates Unified Aerosol Experiment: UAE2. NRL Report Nr. NRL/MR/7534–05-8899, pp 105–110.

Deschamps, P.Y., F.-M. Breon, M. Leroy, A. Podaire, A. Bricaud, J.C. Buriez, and G. Seze, 1994, The POLDER Mission : Instrument characteristics and scientific objectives. IEEE Trans Geosci Remote Sens., 2, 598–615.

Deuzé, J.L., F.-M. Breon, P.Y. Dechamps, C. Devaux, M. Herman, A. Podaire and J.L. Roujean, 1993, Analysis of the POLDER (POLarization and Directionnality of Earth's Reflectances) Airborne Instrument Observations over Land Surfaces. Remote Sens. Environ., 45, 137–154.

Dinter, T., W. von Hoyningen-Huene, J.P. Burrows, A. Kokhanovsky, E. Bierwirth, M. Wendisch, D. Müller, R. Kahn, and M. Diouri, 2009. Retrieval of aerosol optical thickness for desert conditions using MERIS observations during SAMUM campaign. Tellus 61B (2009), 220–237.

Dubovik, O., A. Smirnov, B.N. Holben, M.D. King, Y.J. Kaufman, T.F. Eck, and I. Slutsker, 2000, Accuracy assessments of aerosol optical properties retrieved from AERONET sun and sky-radiance measurements. J. Geophys. Res, 105, 9791–9806.

Dubovik, O., B.N. Holben, T.F. Eck, A. Smirnov, Y.J. Kaufman, M.D. King, D. Tanré and I. Slutsker, 2002, Variability of Absorption and Optical Properties of Key Aerosol Types Observed in Worldwide Locations. J. Atmos. Sci 59, 590–698.

Dubovik O., A. Sinyuk, T. Lapyonok, B.N. Holben, M. Mishchenko, P. Yang, T.F. Eck, H. Volten, O. Munoz, B. Veihelmann, W.J. van der Zande, J.-F. Leon, M. Sorokin and I. Slutsker, 2006, Application of spheroid models to account for aerosol particle nonsphericity in remote sensing of desert dust. J. Geophys. Res., 111, D11208, doi:10.1029/2005JD006619.

Eck, T.F., B.N. Holben, J.S. Reid, O. Dubovik, A. Smirnov, N.T. O'Neill, I. Slutsker, and S. Kinne, 1999, Wavelength dependence of the optical depth of biomass burning, urban, and desert dust aerosol. J. Geophys. Res., 104, 31 333–31 350.

Engel-Cox, J.A., C.H. Holloman, B.W. Coutant and R.M. Hoff, 2004, Qualitative and quantitative evaluation of MODIS satellite sensor data for regional and urban scale air quality. Atmos. Environ., 38, 2495–2509.

Engel-Cox, J.A., R.M. Hoff, R. Rogers, F. Dimmick, A.C. Rush, J.J. Szykman, J. Al-Saadi, D.A. Chu, E.R. Zell, 2006, Integrating lidar and satellite optical depth with ambient monitoring for 3-D dimensional particulate characterisation. Atmos. Environ., 40, 8056–8067.

Fernald, F.G., B.M. Herman and J.A. Reagan, 1972, Determination of aerosol height distributions with lidar. J. Appl. Meteorol., 11, 482–489.

Flowerdew R.J., and J.D. Haigh, 1995, An approximation to improve accuracy in the derivation of surface reflectances from multi-look satellite radiometers. Geophys. Res. Lett., 23, 1693–1696.

Grey, W.M.F., P.R.J. North, S.O. Los and R.M. Mitchell, 2006, Aerosol optical depth and land surface reflectance from multi-angle AATSR measurements: Global validation and inter-sensor comparisons. IEEE Trans. Geosci. Remote Sens., 44, 2184–2197.

Griggs, M., 1975, Measurements of atmospheric aerosol optical thickness over water using ERS-1 data. J. Air Pollut. Conlrol. Assoc., 25, 622–626.

Hasekamp, O.P., and J. Landgraf, 2005, Retrieval of aerosol properties over the ocean from multispectral single-viewing-angle measurements of intensity and polarization: Retrieval approach, information content, and sensitivity study. J. Geophys. Res., 110, D20207, doi:10.1029/2005JD006212.

Herman M., J.-L. Deuzé, A. Marchand, B. Roger, P. Lallart (2005), Aerosol remote sensing from POLDER/ADEOS over the ocean: Improved retrieval using a nonspherical particle model, J. Geophys. Res., **110**, D10S02, doi:10.1029/2004JD004798.

Hess, M., P. Koepke and I. Schult, 1998, Optical properties of aerosols and clouds : The software package OPAC. Bull. Am. Met. Soc., **79**, 831–844.

Höller, R., P. Garnesson, C. Nagl, and T. Holzer-Popp, 2007, Using satellite aerosol products for monitoring national and regional air quality in Austria. Proc. 'Envisat Symposium 2007', Montreux, Switzerland, 23–27 April 2007 (ESA SP-636).

Holben, B., T. Eck, I. Slutsker, D. Tanre, J. Buis, E. Vermote, J. Reagan, Y. Kaufman, T. Nakajima, F. Lavenau, I. Jankowiak and A.Smirnov, 1998, AERONET, a federated instrument network and data-archive for aerosol characterization. Rem. Sens. Environ., **66**, 1–66.

Holben, B.N., D. Tanré, A. Smirnov, T.F. Eck, I. Slutsker, N. Abuhassan, W.W. Newcomb, J.S. Schafer, B. Chatenet, F. Lavenu, Y.J. Kaufman, J.V. de Castle, A. Setzer, B. Markham, D. Clark, R. Froin, R. Halthore, A. Karnieli, N.T. O'Neill, C. Pietras, R.T. Pinker, K. Voss and G. Zibordi, 2001, An emerging ground-based aerosol climatology: Aerosol optical depth from AERONET. J. Geophys. Res., **106**, 12.067–12.097.

Holzer-Popp, T., M. Schroedter and G. Gesell, 2002, Retrieving aerosol optical depth and type in the boundary layer over land and ocean from simultaneous GOME spectrometer and ATSR-2 radiometer measurements, 1, Method description. J. Geophys. Res., **107**, 4578, doi:10.1029/2001JD002013.

Hunt W. H., D. M. Winker, M. A. Vaughan, K. A. Powell, P. L. Lucker, C. Weimer, 2009, CALIPSO lidar description and performance assessment. J. Atmos. Oceanic Technol., **26**, 1214–1228, doi: 10.1175/2008JTECHA1221.1.

Hutchison, K.D., 2003, Applications of MODIS satellite data and products for monitoring air quality in the state of Texas. Atmos. Environ., **37**, 2403–2412.

IPCC, 2007: Climate Change 2007: The Physical Science Basis. Contribution of Working Group I to the Fourth Assessment Report of the Intergovernmental Panel on Climate Change, In: S. Solomon, D. Qin, M. Manning, Z. Chen, M. Marquis, K.B. Averyt, M. Tignor and H.L. Miller (editors), Cambridge University Press, Cambridge, United Kingdom and New York, NY, USA, 996 pp.

Ichoku, C., L.A. Remer and T.F. Eck, 2005, Quantitative evaluation and intercomparison of morning and afternoon Moderate Resolution Imaging Spectroradiometer (MODIS) aerosol measurements from Terra and Aqua. J. Geophys. Res., **110**, D10S03, doi:10.1029/2004JD004987.

Kacenelenbogen, M., J.-F. Léon, I. Chiapello, and D. Tanré, 2006, Characterization of aerosol pollution events in France using ground-based and POLDER-2 satellite data. Atmos. Chem. Phys., **6**, 4843–4849.

Kahn, R. A., W.-H. Li, C. Moroney, D. J. Diner, J. V. Martonchik, and E. Fishbein, 2007, Aerosol source plume physical characteristics from space-based multiangle imaging. J. Geophys. Res., **112**, D11205, doi:10.1029/2006JD007647.

Kahn, R.A., D.L. Nelson, M.J. Garay, R.C. Levy, M.A. Bull, D.J. Diner, J.V. Martonchik, S.R. Paradise, E.G. Hansen and L.A. Remer, 2009, MISR Aerosol Product Attributes and Statistical Comparisons With MODIS. IEEE Trans. On Geosc. and Remote Sensing, **47**, 4095–4114.

Katsev, I.L., A.S. Prikhach, E.P. Zege, A.P. Ivanov and A.A. Kokhanovsky, 2009, Iterative procedure for retrieval of spectral optical thickness and surface reflectance from satellite data using fast radiative transfer code and its application to MERIS measurements, in: A.A. Kokhanovsky and G. de Leeuw (editors) Satellite Aerosol Remote Sensing Over Land, Springer, Berlin, 101–132.

Kaufman, Y., A. Smirnov, B. Holben and O. Dubovik, 2001, Baseline maritime aerosol: methodology to derive the optical thickness and scattering properties. Geophys. Res. Letters, **28**, 3251–3254.

Kaufman, Y.J, D. Tanré and O. Boucher, 2002, A satellite view of aerosols in the climate system. Nature **419**, 215–223.

Kinne, S., 2009, Remote Sensing Data Combinations – Superior Global Maps for Aerosol Optical Depth, in: A.A. Kokhanovsky and G. de Leeuw (editors) Satellite Aerosol Remote Sensing Over Land, Springer, Berlin, 361–381.

Kinne, S., M. Schulz, C. Textor, S. Guibert, S. Bauer, T. Berntsen, T. Berglen, O. Boucher, M. Chin, W. Collins, F. Dentener, T. Diehl, R. Easter, J. Feichter, D. Fillmore, S. Ghan, P. Ginoux, S. Gong, A. Grini, J. Hendricks, M. Herzog, L. Horowitz, I. Isaksen, T. Iversen, D. Koch, M. Krol, A. Lauer, J.F. Lamarque, G. Lesins, X. Liu, U. Lohmann, V. Montanaro, G. Myhre, J. Penner, G. Pitari, S. Reddy, O. Seland, P. Stier, T. Takemura and X. Tie, An AeroCom initial assessment – optical properties in aerosol component modules of global models. ACP, **6**, 1–22, 2006.

Klett, J.D., 1985, Lidar inversion with variable backscatter/extinction ratios. Applied Optics, **24**, 1638–1643.

Koepke, P., 1984, Effective reflectance of oceanic whitecaps. Appl. Opt., **23**, 1816–1824.

Kokhanovsky, A.A., and G. de Leeuw, 2009, Satellite Aerosol Remote Sensing Over Land. Springer, Berlin.

Kokhanovsky, A.A., F.-M. Breon, A. Cacciari, E. Carboni, D. Diner, W. Di Nicolantonio, R.G. Grainger, W.M.F. Grey, R. Höller, K.-H. Lee, Z. Li, P.R.J. North, A.M. Sayer, G.E. Thomas and W. von Hoyningen-Huene, 2007, Aerosol remote sensing over land: A comparison of satellite retrievals using different algorithms and instruments. Atmospheric Research, **85**, 372–394.

Kokhanovsky, A.A., R. L. Curier, Y. Bennouna, R. Schoemaker, G. de Leeuw, P.R.J. North, W. M. F. Grey, K.-H. Lee, 2009, The inter-comparison of AATSR dual view aerosol optical thickness retrievals with results from various algorithms and instruments, *Int. J. Remote Sensing*, 30: **17**, 4525–4537, 10.1080/01431160802578012.

Koren, I., L.A. Remer, Y.J. Kaufman, Y. Rudich and J.V. Martins, 2007, On the twilight zone between clouds and aerosols. Geophys. Res. Lett., **34**, L08805, doi:10.1029/2007GL029253, 2007.

Lee, K. H., Z. Li, Y.J. Kim and A.A. Kokhanovsky, 2009, Aerosol monitoring from satellite observations: a history of three decades. In: Y.J. Kim, U. Platt, M.B. Gu and H. Iwahashi (Editors). Atmospheric and Biological Environmental Monitoring, Berlin: Springer, 13–38.

Lenoble, J., M. Herman, J. Deuzé, B. LaFrance, R. Santer and D. Tanré, 2007, A successive order of scattering code for solving the vector equation of transfer in the Earth's atmosphere with aerosols. J. Quant. Spectrosc. Radiat. Transf., **1007**, 479–507.

Levy, R.C., L.A. Remer and O. Dubovik, 2007a, Global aerosol optical properties and application to Moderate Resolution Imaging Spectroradiometer aerosol retrieval over land. J. Geophys. Res., **112**, D13210, doi:10.1029/2006JD007815.

Levy, R.C., L.A. Remer, S. Mattoo, E.F. Vermote and Y.J. Kaufman, 2007b, Second-generation operational algorithm: Retrieval of aerosol properties over land from inversion of Moderate Resolution Imaging Spectroradiometer spectral reflectance. J. Geophys. Res., **112**, D13211, doi:10.1029/2006JD007811.

Liu, L., and M.I. Mishchenko, 2008, Toward unified satellite climatology of aerosol properties: direct comparisons of advanced level 2 aerosol products. J. Quant. Spectrosc. Radiat. Transf., **109**, 2376–2385.

Liu Z., M.A. Vaughan, D.M. Winker, C.A. Hostetler, L.R. Poole, D.L. Hlavka, W.D. Hart and M.J. McGill, 2004, Use of Probability Distribution Functions for Discriminating Between Cloud and Aerosol in Lidar Backscatter Data. J. Geophys. Res., **109**, doi:10.1029/2004JD004732.

Liu Z., A.H. Omar, Y. Hu, M.A. Vaughan, D.M. Winker, L.R. Poole and T.A. Kovacs, 2005, CALIOP Algorithm Theoretical Basis Document Part 4: Scene Classification Algorithms. NASA-CNES document PC-SCI-203.

Liu Z., M. Vaughan, D. Winker, C. Kittaka, B. Getzewitch, R. Kuehn, A. Omar, K. Powell, C. Trepte, and C. Hostetler, 2009, The CALIPSO Lidar Cloud and Aerosol Discrimination: Version 2 Algorithm and Initial Assessment of Performance, J. Atmos. Oceanic Technol., **26**, 1198–1213.

Maignan, F., F.-M. Breòn and R. Lacaze, 2004, Bidirectional reflectance of Earth targets: valuation of analytical models using a large set of spaceborne measurements with emphasis on the Hot Spot. Remote Sens Environ., **90**, 210–220.

McCormick, M.P., P. Hamill, P.J. Pepin, W.P. Chu, T.J. Swissler and L.R. McMaster, 1979, Satellite studies of the Stratospheric aerosol. Bull. American Meteorol. Soc., **60**, 1038–1046.

Mekler, Y., H. Quenzel, G. Ohring and I. Marcus, 1977, Relative atmospheric aerosol content from ERS observations. J. Geophys. Res., **82**, 967–972.

Mercado, L.M., N. Bellouin, S. Sitch, O. Boucher, C. Huntingford, M. Wild and P.M. Cox, 2009, Impact of changes in diffuse radiation on the global land carbon sink. Nature **458**, 1014–1017. doi:10.1038/nature07949

Mie, G., 1908, Beiträge zur Optik trüber Medien, speziell kolloidaler Metallösungen. Ann. Phys., **25**, 377–445.

Mishchenko, M.I., I.V. Geogdzhayev, W.B. Rossow, B. Cairns, B.E. Carlson, A.A. Lacis, L. Liu and L.D. Travis, 2007, Long-term satellite record reveals likely recent aerosol trend. Science 315 (5818), 1543. DOI: 10.1126/science.1136709

Myhre, G., F. Stordal, M. Johnsrud, A. Ignatov, M.I. Mishchenko, I.V. Geogdzhayev, D. Tanré, J.L. Deuzé, P. Goloub, T. Nakajima, A. Higurashi, O. Torres and B.N. Holben, 2004, Intercomparison of satellite retrieved aerosol optical depth over ocean. J. Atmos. Sci., **61**, 499–513.

Myhre, G., F. Stordal, M. Johnsrud, D.J. Diner, I.V. Geogdzhayev, J.M. Haywood, B.N. Holben, T. Holzer-Popp, A. Ignatov, R.A. Kahn, Y.J. Kaufman, N. Loeb, J.V. Martonchik, M.I. Mishchenko, N.R. Nalli, L.A. Remer, M. Schroedter-Homscheidt, D. Tanré, O. Torres, and M. Wang, 2005, Intercomparison of satellite retrieved aerosol optical depth over ocean during the period September 1997 to December 2000. Atmos. Chem. Phys., **5**, 1697–1719.

Nadal, F., and F.-M. Bréon, 1999, Parametrisation of surface polarised reflectance derived from POLDER spaceborne measurements. IEEE Trans. Geosci. Remote Sens., **37**, 1709–1718.

North, P.R.J., C. Brockmann, J. Fischer, L. Gomez-Chova, W. Grey, A. Heckel, J. Moreno, R. Preusker and P. Regner, 2008, MERIS/AATSR synergy algorithms for cloud screening, aerosol retrieval and atmospheric correction. in Proc. 2nd MERIS/AATSR User Workshop, ESRIN, Frascati, 22- 26 September 2008. (CD-ROM), ESA Publications Division, European Space Agency, Noordwijk, The Netherlands.

Omar, A.H., J.-G. Won, S.-C. Yoon, O.D. David, M. Winker and M.P. McCormick, 2004, Development of global aerosol models using cluster analysis of AERONET measurements. J. Geophys. Res., **110**, D10S14, doi:10.1029/2004JD004874.

Omar A. H., D. M. Winker, C. Kittaka, M. A. Vaughan, Z. Liu, Y. Hu, C. T. Trepte, R. R. Rogers, R. A. Ferrare, K.-P. Lee, R. E. Kuehn, and C. A. Hosteler, 2009, The CALIPSO automated aerosol classification and lidar ratio selection algorithm. J. Atmos. Oceanic Technol., **26**, 1994–2014, DOI: 10.1175/2008JTECHA1221.1.

Pal, S.R., W. Steinbrecht and A.I. Carswell, 1992, Automated method for lidar determination of cloud-base height and vertical extent. Applied Optics, 31, 1488–1494.

Platt, C.M.R., 1973, Lidar and radiometer observations of cirrus clouds. J. Atmos. Sci., **30**, 1191–1204.

Powell K. A., C. A. Hostetler, Z. Liu, M. A. Vaughan, R. E. Kuehn, W. H. Hunt, K.P. Lee, C. R. Trepte, R. R. Rogers, S. A. Young and D. M. Winker, 2009, CALIPSO lidar calibration algorithms Part I: Night-time 532-nm parallel channel and 532-nm perpendicular channel. J. Atmos. Oceanic Technol., **26**, 2015–2033, doi: 10.1175/2008JTECHA1221.1.

Quaas J., O. Boucher, N. Bellouin and S. Kinne, 2008, Satellite based estimate of the direct and indirect aerosol climate forcing, J. Geophys. Res., **113**, D05204, doi:10.1029/2007JD008962.

Reagan J. A., X. Wang, and M. J. Osborn, 2002, Spaceborne lidar calibration from cirrus and molecular backscatter returns. IEEE Trans. Geosci. Remote Sens., **40**, 2285–2290.

Reid, J.S., S.J. Piketh, R. Kahn, R.T. Bruintjes and B.N. Holben (Editors), 2005, A Summary of First Year Activities of the United Arab Emirates Unified Aerosol Experiment: UAE2. NRL Report Nr. NRL/MR/7534–05-8899.

Remer, L.A., Y.J. Kaufman, D. Tanré, S. Mattoo, D.A. Chu, J.V. Martins, R.R. Li, C. Ichoku, R.C. Levy, R.G. Kleidman, T.F. Eck, E. Vermote and B.N. Holben, 2005, The MODIS aerosol algorithm, products, and validation. J. Atmos. Sci., **62**, 947–973.

Robles Gonzalez, C., 2003, Retrieval of Aerosol Properties using ATSR-2 Observations and their Interpretation. PhD thesis, University of Utrecht, Utrecht, The Netherlands.

Robles-Gonzalez, C., J.P. Veefkind and G. de Leeuw, 2000, Mean aerosol optical depth over Europe in August 1997 derived from ATSR-2 data. Geophys. Res. Lett. **27**, 955–959.

Robles-Gonzalez, C., G. de Leeuw, R. Decae, J. Kusmierczyk-Michulec, and P. Stammes, 2006, Aerosol properties over the Indian Ocean Experiment (INDOEX) campaign area retrieved from ATSR-2. J. Geophys. Res., **111**, D15205, doi:10.1029/2005JD006184.

Robles-Gonzalez, C., and G. de Leeuw, 2008, Aerosol properties over the SAFARI-2000 area retrieved from ATSR-2. J. Geophys. Res., **113**, D05206, doi:10.1029/2007JD008636.

Rossow, W., A. Walker and C. Garder, 1993, Comparison of ISCCP and other cloud amounts, J. Climate, **6**, 2394–2418.

Santer, R., V. Carrere, P. Dubuisson and J.-C. Roger, 1999, Atmospheric corrections over land for MERIS. Int. J. of Rem. Sens., **20**, 1819–1840.

Santer, R, Carrere, V., Dessailly, D., Dubuisson, P., and Roger, J.-C., 2000: MERIS Algorithm theoretical basis document, ATBD 2.15, Atmospheric corrections over land.

Schaaf, C., F. Gao, A. Strahler, W. Lucht, X. Li, T. Trang, N. Strucknell, X. Zhang, Y. Jin, J.-P. Mueller, P. Lewis, M. Barnsley, P. Hobson, M. Disney, G. Roberts, M. Dunderdale, R. D'Entremont, B. Hu, S. Liang, J. Privette and D. Roy, 2002, First oberservational BRDF, albedo and nadir reflectance from MODIS. Remote Sens. Environ., **83**, 135–148.

Schaap, M., K. Muller and H.M. ten Brink, 2002, Constructing the European aerosol nitrate concentration field from quality analysed data. Atmos. Environ., **36**, 1323–1335.

Schaap, M., R.M.A. Timmermans, R.B.A Koelemeijer, G. de Leeuw and P.J.H. Builtjes, 2008, Evaluation of MODIS aerosol optical thickness over Europe using sun photometer observations. Atmos. Environ., **42**, 2187–2197, doi:10.1016/j.atmosenv.2007.11.044.

Schulz M., C. Textor, S. Kinne, Y. Balkanski, S. Bauer, T. Berntsen, T. Berglen, O. Boucher, F. Dentener, S. Guibert, I.S.A. Isaksen, T. Iversen, D. Koch, A. Kirkevag, X. Liu, V. Montenaro, G. Myhre, J.E. Penner, G. Pitari, S. Reddy, O. Seland, P. Stier and T. Takemura, 2006, Radiative forcing by aerosols as derived from the AeroCom present-day and pre-industrial simulations. ACP, **6**, 5225–5346.

Seinfeld, J.H., and S.N. Pandis, 1998, Atmospheric Chemistry and Physics. Wiley.

Silva, A.M., M.L. Bugalho, M.J. Costa, W.V. Hoyningen-Huene, T. Schmidt, J. Heintzenberg, S. Henning, 2002, Aerosol optical properties from columnar data during the second Aerosol Characterization Experiment an the south coast of Portugal. J. Geophys. Res., **107**, doi: 10.1029/2002JD002196.

Smirnov, A., B.N. Holben, I. Slutsker, D. M. Giles, C. R. McClain, T.F. Eck, S.M. Sakerin, A. Macke, P. Croot, G. Zibordi, P.K. Quinn, J. Sciare, S. Kinne, M. Harvey, T.J. Smyth, S. Piketh, T. Zielinski, A. Proshutinsky, J.I. Goes, N.B. Nelson, P. Larouche, V.F. Radionov, P. Goloub, K. Krishna Moorthy, R. Matarrese, E.J. Robertson, and F. Jourdin, 2009, Maritime Aerosol Network as a component of Aerosol Robotic Network. J. Geophys. Res., **114**, D06204, doi:10.1029/2008JD011257.

Sogacheva, L., P. Kolmonen, L. Curier, G. de Leeuw, A. Kokhanovsky, 2009, Combined AATSR/ MERIS algorithm AMARA for aerosol optical depth retrieval over ocean. Proceedings of OceanObs'09, 21–25 September 2009, Venice, Italy.

Stammes, P., 2001, Spectral radiance modelling in the UV-Visible range. in: W.L. Smith and Y.M. Timofeyev (editors), Current problems in Atmospheric Radiation, A. Deepak Publication, Hampton, VA, pp. 385–388.

Stowe, L.L., H. Jacobowitz, G. Ohring, K.R. Knapp and N.R. Nalli, 2002, The Advanced Very High Resolution Radiometer (AVHRR) Pathfinder Atmosphere (PATMOS) climate dataset: Initial analyses and evaluations. J. Clim., **15**, 1243–1260.

Thomas, G.E., C.A. Poulsen, R. L. Curier, G. de Leeuw, S. H. Marsh, E. Carboni, R. G. Grainger and R. Siddans, 2007, Comparison of AATSR and SEVIRI aerosol retrievals over the Northern Adriatic. QJRM, **133**, 85–95, doi: 10.1002/qj.126.

Torres, O., P.K. Bhartia, J.R. Herman and Z. Ahmad, 1998, Derivation of aerosol properties from satellite measurements of backscattered ultraviolet radiation. Theoretical Basis. J. Geophys. Res., **103**, 17099–17110.

Torres, O., P.K. Bhartia, J.R. Herman, A. Sinyuk and B.N. Holben, 2002, A long term record of aerosol optical thickness from TOMS observations and comparison to AERONET measurements. J. Atm. Sci.,**59**, 398–413.

Torres, O., A. Tanskanen, B. Veihelmann, C. Ahn, R. Braak, P.K. Bhartia, J.P. Veefkind, and P.F. Levelt, 2007, Aerosols and Surface UV Products from OMI Observations: An Overview. J. Geophys. Res., **112**, D24S47, doi:10.1029/2007JD008809.

Vaughan M.A., D. M. Winker, and C.A. Hostetler, 2002, SIBYL: a Selective Iterated Boundary Location Algorithm for Finding Cloud and Aerosol Layers in CALIPSO Lidar Data. In: L. R. Bissonnette, G. Roy and G. Vallée (editors), Lidar Remote Sensing in Atmospheric and Earth Sciences, Defence R&D Canada – Valcartier, Québec, Canada, pp. 791–794.

Vaughan M.A., D.M. Winker and K.A. Powell, 2005, CALIOP Algorithm Theoretical Basis Document Part 3: Feature Detection and Layer Properties Algorithms. NASA-CNES document PC-SCI-203.

Vaughan M., K. Powell, R. E. Kuehn, S. Young, D. M. Winker, C. A. Hostetler, W. H. Hunt, Z. Liu, M. J. McGill and B. J. Getzewitch, 2009, Fully automated detection of cloud and aerosol layers in the CALIPSO lidar measurements. J. Atmos. Oceanic Technol., **26**, 2034–2050, DOI: 10.1175/2008JTECHA1221.1.

Veefkind, J.P. and G. de Leeuw, 1998, A new algorithm to determine the spectral aerosol optical depth from satellite radiometer measurements. J. of Aerosol Sciences, **29**, 1237–1248.

Veefkind, J.P., G. de Leeuw and P.A. Durkee, 1998, Retrieval of aerosol optical depth over land using two-angle view satellite radiometry during TARFOX. Geophys. Res. Lett. **25**, 3135–3138.

Veefkind, J.P., G. de Leeuw, P. Stammes and R.B.A. Koelemeijer, 2000, Regional distribution of aerosol over land derived from ATSR-2 and GOME. Remote sens Environ., **74**,377–386.

Veihelmann, B., P.F. Levelt, P. Stammes and J.P. Veefkind, 2007, Aerosol Information Content in OMI Spectral Reflectance Measurements. Atmos. Chem. Phys., **7**, 3115–3127.

Vermeulen, A., C. Devaux and M. Herman, 2000, Retrieval of the scattering and microphysical properties of aerosols from ground-based optical measurements including polarization. I. Method. Appl. Opt., **39**, 6207–6220.

Verver, G.H.L., J.S. Henzing, G. de Leeuw, C. Robles Gonzalez and P.F.J. van Velthoven, 2002, Aerosol retrieval and assimilation (ARIA). Final report Phase 1, NUSP-2, 02-09, KNMI-publicatie: 200.

Volten, H., O. Munoz, E. Rol, J.F. de Haan, W. Vassen, J.W. Hovenier, K. Muinonen and T. Nousiainen, 2001, Scattering matrices of mineral aerosol particles at 441.6 and 632.8 nm. J. Geophys. Res., **106**, 17375–17401.

von Hoyningen-Huene, W., and P. Posse, 1997, Non-sphericity of aerosol particles and their contribution to radiative forcing. J.Quant. Spectr. Rad. Trans. **57**, 651–668.

von Hoyningen-Huene, W., K. Wenzel and S. Schienbein, 1999a, Radiative properties of desert dust and its effect on radiative balance. J. Aeros. Sci., **30**, 489–502.

von Hoyningen-Huene, W., T. Schmidt, S. Schienbein, A.K. Chan and J.T. Lim, 1999b, Climate relevant aerosol parameters of South-East Asian forest fire haze. Atm. Env., **33**, 3183–3190.

von Hoyningen-Huene, W., M. Freitag and J.B. Burrows, 2003, Retrieval of aerosol optical thickness over land surfaces from top-of-atmosphere radiance. J. Geophys. Res., **108**, 4260. doi:10.1029/2001JD002018.

von Hoyningen-Huene, W., A.A. Kokhanovsky, J.B. Burrows, V. Bruniquel-Pinel, P. Regner and F. Baret, 2006, Simultaneous determination of aerosol- and surface characteristics from top-of-atmosphere reflectance using MERIS on board ENVISAT. Adv Space Res., **37**, 2172–2177.

von Hoyningen-Huene, W., A.A. Kokhanovsky and J.P. Burrows, 2008, Retrieval of Particulate Matter from MERIS Observations. In: Y.J. Kim and U. Platt, (editors), Advanced Environmental Monitoring. Springer, Berlin, pp. 190–202.

Wang, M., and H.R. Gordon, 1994, Radiance reflected from the ocean-atmosphere system: synthesis from the individual components of the aerosol size distribution. Appl. Opt., **33**, 7088–7095.

Wang J. and S.A. Christopher, 2003, Intercomparison between satellite-derived aerosol optical thickness and PM25 mass: implications for air quality studies. Geophys. Res. Lett., **30**, 2095, doi:10.1029/2003GL018174.

Winker, D.M., R.H. Couch and M.P. McCormick, 1996, An overview of LITE: NASA's Lidar In-space Technology Experiment. Proc. IEEE, **84**, 164–180.

Winker D.M., J.R. Pelon and M.P. McCormick, 2003, The CALIPSO mission: spaceborne lidar for observation of aerosols and clouds, Proc. of SPIE, **4893**, 1–11.

Winker D.M., W.H. Hunt and M.J. McGill, 2007, Initial performance assessment of CALIOP. Geophys. Res. Lett., 34, L19803, doi:10.1029/2007GL030135.

Winker, D.M., M.A. Vaughan, A.H. Omar, Y. Hu, K.A. Powell, Z. Liu, W.H. Hunt, and S.A. Young, 2009., Overview of the CALIPSO Mission and CALIOP Data Processing Algorithms. J. Atmos. Oceanic Technol., **26**, 2310–2323, doi: 10.1175/2008JTECHA1221.1.

Young, S.A., 1995, Lidar analysis of lidar backscatter profiles in optically thin clouds. Appl. Opt., **34**, 7019–7031.

Young S.A., D.M. Winker, V. Noel, M.A. Vaughan, Y.Hu, R.E. Kuehn, 2005, Algorithm Theoretical Basis Document Part 5: Extinction Retrieval and Particle Property Algorithms, NASA-CNES document PC-SCI-203.

Young S. and M. Vaughan, 2009, The retrieval of profiles of particulate extinction from cloud-aerosol lidar infrared pathfinder satellite observations (CALIPSO) data: algorithm description. J. Atmos. Oceanic Technol., **26**, 1105–1119, DOI: 10.1175/2008JTECHA1221.1.

Zwally, H.J., B. Schutz, W. Abdalati, J. Abshire, C. Bentley, A. Brenner, J. Bufton, J. Dezio, D. Hancock, D. Harding, T. Herring, B. Minster, K. Quinn, S. Palm, J. Spinhirne and R. Thomas, 2002, ICESat's laser measurements of polar ice, atmosphere, ocean, and land. J of Geodynamics **34**, 405–445.